Multidisciplinary
Simulation, Estimation, and Assimilation Systems
Reports in Ocean Science and Engineering

MSEAS-05

Upwelling Dynamics off Monterey Bay: Heat Flux and Temperature Variability, and their Sensitivities

by

Melissa Rachel Steinberg Kaufman

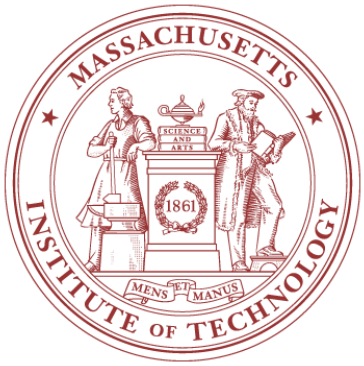

Department of Mechanical Engineering
Massachusetts Institute of Technology

Cambridge, Massachusetts

May 2010

Upwelling Dynamics off Monterey Bay: Heat Flux and Temperature Variability, and their Sensitivities

By

Melissa Rachel Steinberg Kaufman

Submitted to the Department of Mechanical Engineering
in Partial Fulfillment of the Requirements for the Degree of

Bachelor of Science in Mechanical Engineering

at the

Massachusetts Institute of Technology

June 2010

© Massachusetts Institute of Technology
All Rights Reserved

Signature of Author . . . . . .
Department of Mechanical Engineering
May 10, 2010

Certified by . . . . . .
Pierre F. J. Lermusiaux
Associate Professor
Thesis Supervisor

Accepted by . . . . . .
John H. Lienhard V
Collins Professor of Mechanical Engineering
Chairman, Undergraduate Thesis Committee

Upwelling Dynamics off Monterey Bay:
Heat Flux and Temperature Variability, and their Sensitivities

by

Melissa Kaufman

Submitted to the Department of Mechanical Engineering on May 10, 2010
in Partial Fulfillment of the Requirements for the Degree of
Bachelor of Science in Mechanical Engineering

ABSTRACT

Understanding the complex dynamics of coastal upwelling is essential for coastal ocean dynamics, phytoplankton blooms, and pollution transport. Atmospheric-driven coastal upwelling often occurs when strong alongshore winds and the Coriolis force combine to displace warmer surface waters offshore, leading to upward motions of deeper cooler, nutrient-dense waters to replace these surface waters. Using the models of the MIT Multidisciplinary Simulation, Estimation, and Assimilation System (MSEAS) group, we conduct a large set of simulation sensitivity studies to determine which variables are dominant controls for upwelling events in the Monterey Bay region. Our motivations include determining the dominant atmospheric fluxes and the causes of high-frequency fluctuations found in ocean thermal balances. We focus on the first upwelling event from August 1- 5, 2006 in Monterey Bay that occurred during the Monterey Bay 06 (MB06) at-sea experiment, for which MSEAS data-assimilative baseline simulations already existed.

Using the thermal energy (temperature), salinity and momentum (velocity) conservation equations, full ocean fields in the region as well as both control volume (flux) balances and local differential term-by-term balances for the upwelling event events were computed. The studies of ocean fields concentrate on specific depths: surface-0m, thermocline-30m and undercurrent-150m. Effects of differing atmospheric forcing contributions (wind stress, surface heating/cooling, and evaporation-precipitation) on these full fields and on the volume and term-by-term balances are analyzed. Tidal effects are quantified utilizing pairs of simulations in which tides are either included or not. Effects of data assimilation are also examined.

We find that the wind stress forcing is the most important dynamical parameter in explaining the extent and shape of the upwelling event. This is verified using our large set of sensitivity studies and examining the heat flux balances. The assimilation of data has also an impact because this first upwelling event occurs during the initialization. Tidal forcing and, to a lesser extent, the daily atmospheric and data assimilation cycles explain the higher frequency fluctuations found in the volume averaged time rate of change of thermal energy.

Thesis supervisor: Pierre Lermusiaux
Title: Associate Professor of Mechanical Engineering

Acknowledgements

I would like to extend my gratitude to Professor Pierre Lermusiaux for his guidance and support. I would also like to thank the rest of the MSEAS group for their help and good humor. I would like especially to thank Pat Haley for his help using the MSEAS software, Wayne Leslie for always having the information I needed, and Matt Ueckermann for patiently answering my numerous questions.

I could not have done this without the encouragement and support from my family and friends. Mom, thank you for reading every draft and always being there. Jonathan, thanks for the encouragement when I needed it most. I am lucky to be surrounded by such an amazing group of friends and colleagues.

We thank the Office of Naval research for supporting the MSEAS group in its "Adaptive Sampling and Prediction (ASAP)" research in the Monterey Bay region under grant "N00014-04-1-0534 – MIT-sub (00000917)" to the Massachusetts Institute of Technology. I would also like to thank Mr. B. Jamieson and the other donors to the Paul E. Gray Endowed Fund for UROP.

Table of contents

List of figures

List of tables

1 Introduction

Upwelling is an important but complex phenomenon occurring in multiple forms in the ocean. Coastal atmospheric-driven upwelling occurs when strong alongshore winds and the Coriolis force combine to displace warmer surface waters offshore, leading to upward motions of deeper cooler, nutrient-dense waters to replace these surface waters. In the Monterey Bay region, relaxation occurs when the winds subside or reverse, and the internal ocean dynamics (e.g. the California Current System) controls the region.

My thesis investigates the thermal (internal) energy and momentum balances associated with the varying types of upwelling and relaxation events of the extended Monterey Bay region, California. To do so, we conduct a large set of sensitivity studies using the ocean models and software of the Multidisciplinary Simulation, Estimation and Assimilation System (MSEAS) group. Our focus is on upwelling and relaxation events sampled during the summer of 2006 as part of the Monterey Bay 06 (MB06) at-sea experiment, for which MSEAS data-assimilative baseline simulations already existed.

Using the thermal energy (temperature), our full ocean field comparisons concentrate on specific depths: surface-0m, thermocline-30m and undercurrent-150m. Effects of differing atmospheric forcing contributions (wind, surface heating, and evaporation-precipitation, and radiation) on these full fields as well as on the volume and term-by-term balances are analyzed. Tidal effects are examined utilizing pairs of simulations in which tides are either included or not. Effects of data assimilation are also quantified. Important questions that motivate our research are: which of the surface wind-stress flux, atmospheric pressure or surface heat fluxes are the main drivers of upwelling events in the region?; ii) are the higher-frequency flux variability observed in our simulations due to tidal and inertial effects, daily atmospheric cycles or data assimilation cycles?; and iii) what are the roles of the internal ocean dynamics and background state during such events, and does this variability in the background ocean sets up the different types of upwelling and relaxation events observed at sea? A final and important motivation is that the results of our studies will allow us to create better computational and theoretical models of three-dimensional and time-dependent upwelling by determining which variables need to be finely tuned for computations and which variables need to be accounted for in theories.

Chapter 2 provides a background on upwelling, a review of studies on upwelling in Monterey Bay, and a summary of the two real-time at-sea experiments with which MSEAS has been involved. Chapter 3 outlines the MSEAS primitive equation model and looks at the sensitivity studies. Chapter 4 examines the first upwelling event in more detail for each of the sensitivity runs by studying and comparing their lateral and surface heat fluxes as well as their volume-averaged time rate of change of temperature. Chapter 5 reviews and summarizes the results.

2 Background

Monterey Bay is a highly studied region due to its strong upwelling season, interesting bathymetry including the Monterey Submarine Canyon, and complex currents. In this chapter, we briefly explain upwelling which is a phenomenon in which cooler, denser water is brought to the surface as a result of along-shore wind stress in coastal regions. We also overview the many studies on upwelling that have been conducted in Monterey Bay. We then discuss the two major at-sea experiments that the MSEAS group has been part of in the region, the Autonomous Ocean Sampling Network-II experiment (AOSN-II) and the Monterey Bay 2006 (MB06) experiment, in closer detail.

2.1 Upwelling

Upwelling is a phenomenon in which cooler, denser water is brought to the surface. There are a few types of upwelling: coastal, equatorial, topographic and along the ice edge. In coastal regions, wind-driven upwelling is the result of an along-shore wind stress and it interacts with the Earth's rotation and turbulent viscous stress. In the surface Ekman layer, as the result of these stresses, the net transport is 90 degrees to the right of the wind in the northern hemisphere and to the left in the southern hemisphere. This 90 degree rotation between wind direction and mean transport is due to the Coriolis effect itself, a result of the rotation of the earth. If the coast is to the left in the Northern Hemisphere or to the right in the Southern Hemisphere, as the surface water is advected upward offshore, due to conservation of mass, the deeper, cooler water is "upwelled" to the surface, as in Figure 2-1.

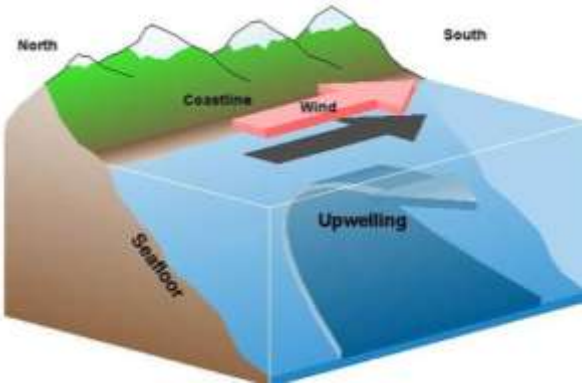

Figure 2-1: Schematic of Coastal Upwelling.
(http://www.greenseaupwelling.com/_images/upwellPic.png)

Upwelling plays an important role in marine biology. For phytoplankton blooms to occur, two conditions must be met: sunlight and nutrients. Both of these conditions are met when the deeper, nutrient rich water is upwelled to the surface, where the sun can reach. Coastal regions with sustained wind-driven upwelling are thus often sites of large fisheries. Upwelling is also important to understand and characterize for specific regions since they can dominate the flows. This is challenging for complex upwelling dynamics that is time and 3-D in space dependent. Finally, upwelling can also be important for studying and predicting pollution transport.

In classical descriptions, upwelling is traditionally modeled as a two-dimensional process, with an absence of alongshore variation. The equations (Cushman-Roisin and Beckers, 2010) for the two-layer, shallow water ocean model are:

$$\frac{\partial u}{\partial t} + u\frac{\partial u}{\partial x} - fv = -g'\frac{\partial h}{\partial x} \tag{2-1}$$

$$\frac{\partial v}{\partial t} + u\frac{\partial v}{\partial x} + fu = \frac{\tau}{\rho_0 h} \tag{2-2}$$

$$\frac{\partial h}{\partial t} + \frac{\partial}{\partial x}(hu) = 0 \tag{2-3}$$

where u and v are the velocities in the cross-shore and alongshore directions, t is time, x is the offshore coordinate, τ is the alongshore wind stress, f is the Coriolis parameter, g' is the reduced gravity due to the density difference between the two layers ($g' = \frac{\Delta\rho}{\rho_0} g$), h is the depth of the fluid, and ρ_0 is the average density of the two layers.

However, in the real world, upwelling is usually a three-dimensional process due to alongshore advection and the three equations above do not account for all of the dynamics. This is why in our study we employ a four-dimensional ocean modeling approach to characterize wind-driven upwelling dynamics.

Upwelling can also be due to topographic effects (topography leading to upward fluid motions). Upwelling can also occur in non-coastal areas. Equatorial upwelling occurs due to the opposite directions of Ekman drift in the two hemispheres. Upwelling can also occur at high latitudes along the ice edge due to the different wind stress on ice and open water. The rest of this document will focus on coastal upwelling in Monterey Bay.

2.2 Literature review

Monterey Bay has been highly studied since it is an area of interesting dynamics due to its uneven sea floor (Monterey Submarine Canyon) and upwelling-favorable winds. It has also been selected due to its "close proximity to several large research institutions, ship availability, and the wealth of environmental and scientific problems presented" (Ramp et al., 2009). Many experiments have been conducted there, including the Coastal Ocean Dynamics Experiment in 1981-1982 (Kelly, 1985; Lentz, 1987; Send et al., 1987), the Shelf Mixed Layer Experiment (SMILE) and Sediment Transport Events over Shelf and Slope (STRESS) in December 1988-1989 (Dever and Lentz, 1994), Rosenfeld et al. (1994) in spring and summer of 1989, Storlazzi et al. (2003) in June 2000-July 2001, Drake et al. (2005)in June 2001-September 2002, Autonomous Ocean Sampling Network-II (AOSN-II) in August-September of 2003 (Haley et al., 2009; Ramp et al., 2009; Shulman et al., 2009) and Monterey Bay 2006 (MB06). A recent review of the dynamics and major features of the California Current System including the Monterey Bay region is being prepared by Gangopadhyay et al. (2010a), including models for most of these features (Gangopadhyay et al., 2010b).

Three distinct seasons have been observed in Monterey Bay, an upwelling favorable summer season, a storm season in the winter, and a spring transition season (Storlazzi et al., 2003). In the spring-summer season, the wind is predominantly stronger coming from the northwest. These winds are due to a region of high pressure off-shore known as the California High. Largier (1993) found that the summer season was characterized by the southwesterly mean wind stress, cold water near the coast, upward tilting isotherms, and a mean equatorward shelf current with strong vertical shear. The alongshore component of the current was highly correlated with local wind stress at all depths over the shelf. The wind stress curl adjacent to the coast is positive (cyclonic) and largest in the summer (Rosenfeld, 1994). In the spring and summer, near surface water offshore Monterey Bay flows southward due to the local equatorward wind stress and the influence of the California Current (Rosenfeld, 1994). Drake (2005) found that the upwelling was most pronounced within a distance of the coast equal to the baroclinic Rossby radius, roughly within 10 km of the shoreline. Rosenfeld (1994) found that the wind driven coastal upwelling affect the upper 100-200 meters.

Usually upwelling is presented as a symmetric two-dimensional process (Sect 2.1); however, Send (1987) found that warming during relaxation is not simply the reverse of cooling during upwelling caused by offshore and vertical advection of cold water; the net surface heat flux also plays an important role. Rudnick and Davis (1988) show that upwelling is not just 2-D because real upwelling are also affected by alongshore gradients and vertical flow associated with mixing. However, Lentz found that the two dimensional Ekman model of upwelling reproduced the major features of fluctuations of offshore heat flux with a correlation of 0.82.

One aspect of upwelling in the Monterey Bay region that has been studied extensively is the thermal energy balance (first law of thermodynamics), referred to in ocean studies as the "heat balance" or "heat budget." Dever and Lentz (1994) found that the changes in heat content integrated over the cross-shelf area were due to cross-shelf advection through the offshore side, along-shelf heat flux divergence due to the volume flux divergence and the temperature gradient flux, and the net surface heat flux. Lentz (1987) found that the largest terms in the heat budget are warming due to net surface heat flux and cooling due to the mean offshore flow of warm surface water and onshore flow of colder deep water. For the summer of 1982 using the CODE-II data set, Lentz found a surface heat transfer rate of $1.6\ 10^{11}$ W into the ocean, and an offshore heat transfer rate of $2.4\ 10^{11}$ W mostly due to the offshore flow of relatively warm water in the upper 30 m. He found that the fluctuations were large relative to the mean, and the primary source of uncertainly in the mean heat budget was resolving the cross-shelf heat flux. The average net surface heat flux during the upwelling season during 1981-1982 was 180 W/m^2. The neat surface heat flux is mostly the result of incident solar radiation. Send (1987) found that 50-60% of the relaxation warming could be attributed to the net surface heat flux. Rudnick and Davis (1988) found a similar value for surface heat flux of 181 W/m^2.

Another aspect studied in the literature is the effects of the tides on the flow field. The temperature spectrum is dominated by diurnal and semi-diurnal tides. Semi-diurnal alongshore currents dominate the flow, and there is a correlation between the semi-diurnal tide and temperature fluctuations (Storlazzi, 2003**)**. Rosenfeld (2009) and Wang (2009) showed that although barotropic tidal currents in Monterey Bay are small, barotropic tides are important on the shelf, with magnitudes of 15-30 cm/s, comparable in magnitude to those associated with California Current eddies and meanders and local coastal upwelling jets. In addition to barotropic tides, internal tides are the result of the Monterey Submarine Canyon, which can generate and trap baroclinic tides and waves.

Monterey Bay is known for its complex ocean topography; the Monterey Bay Canyon and many capes further complicate the dynamics of the area Largier(1993) found that shelf topography plays an important role in upwelling; the upwelling was enhanced to the south of Cape Mendocino and suppressed immediately to the north. He also noted the presence of a persistent mesoscale anticyclonic eddy abutting the shelf during the upwelling season that would likely affect the smaller alongshore scales. Kelly (1985) found similar results: she found that the "irregular coastline generates irregular upwelling patterns in response to spatially uniform wind stress." She also found that the upwelling plumes were anchored to the coastal topography, especially capes, at least over the coast. However, not everyone agrees that the upwelling is related to the Monterey Canyon; Rosenfeld (1994) believes that the water is upwelled at a remote site and subsequently advected into the Bay. Using data collected and model simulations for the spring-summer season in 1989, they found that at least 70% of the water in the upper 30 m must have been

replaced between June 20th and June 29th to lower the salinity to match the observation, and the water must be advected from the California Current meander west of the Bay.

The wind is not always consistently in the upwelling-favorable direction, and the heat balance and dynamics are different in this situation, also known as a relaxation event. Send (1987) found that the flow was over the shelf to the north in the absence of alongshelf winds. The wind relaxations led the inner shelf currents to reverse direction and flow poleward. The alongshelf advection and surface heat flux together accounted for most of the observed warming. Alongshelf advection of warm water into the area from farther south may occur once the alongshelf flow is reversed. This can be seen in sea surface temperature from satellite images, infrared images, and chlorophyll concentration tracer. Low salinity values also support the origin of the water from the south of the Monterey area, as found by CODE (Send et al., 1987).

In the next section, we will focus on AOSN-II and MB06 in more detail due to the involvement of the MSEAS group in these two multi-institutional exercises.

2.3 MSEAS Modeling Experiments

The MSEAS group has been involved with two experiments in the Monterey Bay region: the AOSN-II and MB06 experiments (Haley et al., 2009; http://www.mbari.org/aosn/MontereyBay2003/). One of their goals was to achieve a better understanding of upwelling, especially in the context of the California Coast. Another goal was to improve numerical models. A third objective was to utilize data-assimilative models to guide the ocean sampling in real-time in an optimal way. In what follows, we describe these two real-time at-sea experiments in a chronological order.

2.3.1 Autonomous Underwater Sampling Network-II (AOSN-II) Sea Experiment

The AOSN-II (Autonomous Ocean Sampling Network-II) experiment occurred during August-September 2003 in Monterey Bay. Its specific goals were to:

- Observe and predict the development and movement of upwelling fronts and ocean eddies
- Determine the importance of the wind-stress curl in driving upwelling and the three-dimensional circulation in the Monterey Bay
- Study the relationship between micro-scale atmospheric jets and the formation of oceanic cold plumes off coastal headlands and promontories
- Examine the nutrient supply process in Monterey Bay including upwelling, advection, and mixing
- Evaluate and improve the numerical models of both the atmosphere and coastal ocean (Ramp et al., 2009).

AOSN-II provided a description of the features of the Bay and a better understanding of the strengths and limitations of forecasts using various skill metrics.

Forecasts were forced using 3 km hourly ocean-atmosphere flux predictions obtained from COAMPS (Coupled Ocean/Atmosphere Mesoscale Prediction System) (COAMPS, Doyle et al., 2009). The numerical model used included two-way nesting capabilities for simulations, with a smaller "data domain" and a larger "off shore domain." There were three configurations for the model: a stand-alone data domain with optimal interpolation methods for data assimilation, a two-way nested domain with objective analysis, and a stand-alone data domain with data assimilation using the ESSE (Error Subspace Statistical Estimation) scheme (Haley et al., 2009). There were no tidal forcings or river inputs in these simulations because the older HOPS modeling system was not capable of such simulations.

The main features found are illustrated on Figure 2-2. The model simulation results included features such as upwelling centers at Point Ano Nuevo and Point Sur where the upwelled water was advected equatorward and seaward. Model output also showed evidence of a coastal current, eddies, squirts and filaments, including upwelling induced jets and high sub-mesoscale variability in the coastal transition zone. At 30 m depth, the data-assimilative simulations showed cyclonic circulation and southward coastal currents along-shelf and across the mouth of Monterey Bay. Offshore, the inflow in the western boundary bent north and provided general northward flow, indicative of a surfacing undercurrent, known as the "Davidson Current." Inshore of this flow, but off the shelf, an anticyclonic eddy was usually present. The winds dominated at the surface, resulting in general southward flow across the whole domain. A band of warmer water lined the coast at the surface, occasionally protruding out the northern edge of the mouth of the bay. At 200 meters, a general northward flow originating from the western boundary was evidenced, sometimes with a northward branch along the slope. The anticyclonic eddy was still present.

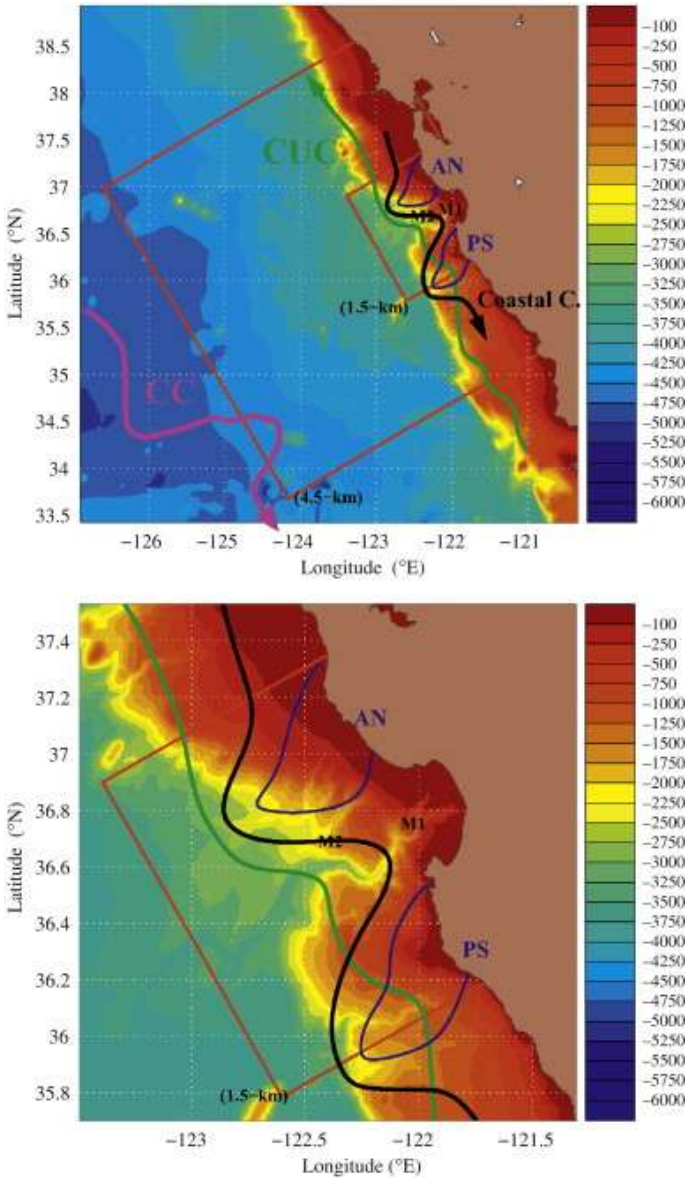

Figure 2-2: Modeling domains for AOSN-II with bathymetry. Upper panel shows the "Data Domain" inside of the larger "Offshore Domain". Lower panel shows a zoom of the "Data Domain". Also shown are the main dynamical features: upwelling centers at point Año Nuevo (AN) and Point Sur (PS) (blue); coastal current, eddies, filaments, etc. (black); California Undercurrent (CUC) (green); California Current (CC) (magenta). (Lermusiaux, 2006; Haley et al., 2009).

The forecast fields were evaluated using root-mean-square (RMS) error and RMS persistence error estimates. On average, the ocean temperature and salinity forecasts had skill out to two days. One-day forecast mean temperature differences showed a correlation with the wind. The temperature and salinity RMS showed both greater skill and variability near the surface than at depth. A third skill metric was also used to test the accuracy of the forecasts: pattern correlation coefficient, also known as anomaly correlation coefficient, a measure based on the correlation of anomalies from the large-scale mean. Using this metric, it was found that temperature and salinity forecasts had skill out to two days. Reanalysis was used to improve long-term robustness by the use of time-varying boundary data, to smooth the topography, and to weaken the relaxation parameters used in the boundary condition scheme. In addition, coastal friction was weakened by increasing the relaxation time-scale. These changes led to improved skill, especially in the thermocline (Haley et al., 2009). Overall, these data-assimilative modeling studies showed two distinct upwelling patterns: the first type of upwelling led to wide westward plumes at Ano Nuevo and Point Sur, while the second type the upwelling front was relatively parallel to the coast, just west of the mouth of Monterey Bay. During strong upwelling events, flow in the upper 10 to 20 meters had scales similar to atmospheric scales with broad features. Once the wind subsided, kinetic energy decayed and led to the development of mesoscale features within a warming upper thermocline. Shulman (2009) researched the impact of glider temperature and salinity observations on the Navy Coastal Ocean Model (NCOM). They found that the model reproduced the observed sequence of events and was in good agreement during upwelling due to good wind agreement; the differences were more substantial during periods of relaxation. They found that once the data assimilation stopped, the forecast was only good out 1-1.5 days, but there was still improvement in hindcasts and nowcasts. To produce better longer forecasts, they needed to have more accurate atmospheric forcings (Shulman, 2009). These results are utilized to guide our research in Chapters 3 and 4.

2.3.2 Monterey Bay 2006 (MB06) Sea Experiment

In mid-July to mid-September 2006, another set of experiments was conducted in Monterey Bay, known as MB06. Figure 2-3 shows the area of the project and the two domains of interest. The small domain had a resolution of 500 m and the large domain had a resolution of 1.5 km. Our sensitivity and upwelling dynamics research utilized MB06 model simulations. In what follows, we describe the goals of MB06, in particular those of the Adaptive Sampling and Prediction (ASAP) team. We also provide our own description of the features and events that occurred at sea, which are results we obtained in collaboration with the MIT-MSEAS group.

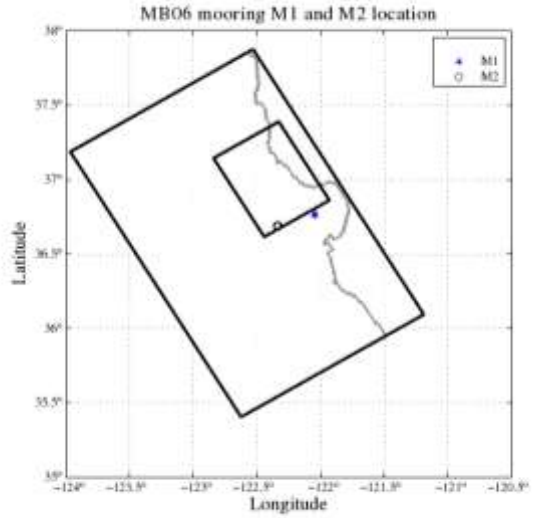

Figure 2-3: MB06 Domain with Mooring Locations. The two outlined rectangles are the nested domains (Heubel, 2008).

Four large experiments were conducted with funding mostly from the Office of Naval Research. These were ASAP (Adaptive Sampling and Prediction), AESOP (Assessing the Effects of Submesoscale Ocean Parameterizations), LOCO (Layered Organization in the Coastal Ocean), and UPS (Undersea Persistent Surveillance). Our focus here is mainly ASAP (http://mseas.mit.edu/Research/ASAP/index.html). The goals of ASAP were to:

- Find the most efficient way of fusing autonomous ocean vehicles such as undersea gliders to study ocean processes associated with the upwelling of cold, deep water along the Central California Coast
- Use the real-time data gathered by autonomous vehicles and other oceanographic instruments to improve computer models of ocean circulation
- Refine these computer models so that they can reliably predict complex processes such as upwelling-related currents.

Data were collected from several research vessels and AUVs (both propeller-driven and gliders), as well as satellites, buoys, airplanes, and drifters. There were 6 SIO Spray gliders and 4 WHOI Slocum gliders. The Princeton Glider Coordinated Control System (GCCS) was used for path planning to steer a fleet of underwater gliders to a set of coordinated trajectories. Figure 2-4 shows the locations and sources of data collected throughout the experiment.

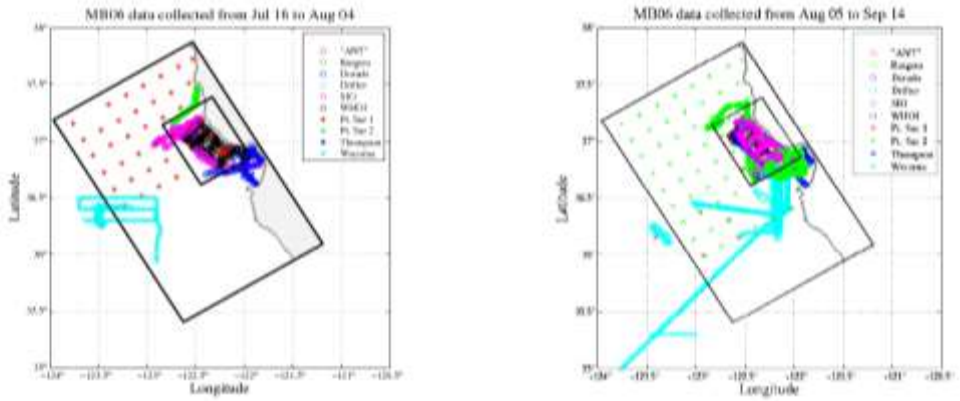

Figure 2-4: Types/Areas of Data Collection. A: July 16-August 4, B: August 5-September 14 (Heubel, 2008).

Several upwelling events occurred during this time period. Figure 3-4 shows the direction from which the wind was blowing at mooring M1 (See Figure 2-3 for location). Periods of strong wind from the north generally correlate well with upwelling events.

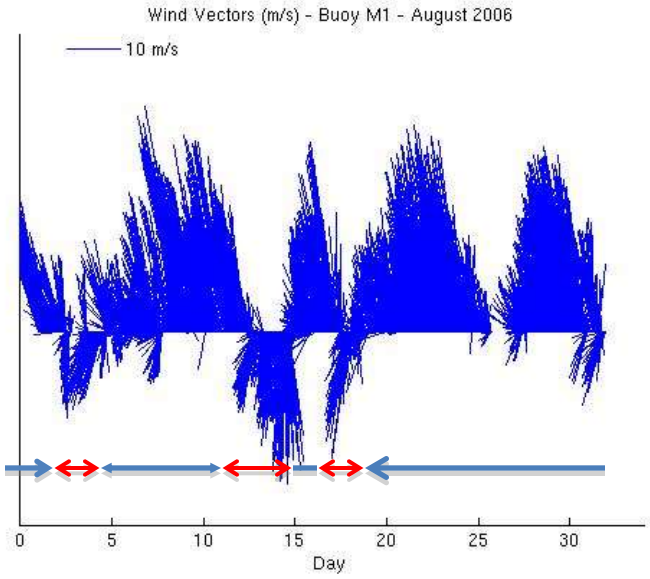

Figure 2-5: Observed Wind for August 2006 at Buoy M1. The blue arrows show periods during which winds are upwelling favorable, while the red arrows show periods during which winds are relaxation favorable (MSEAS group, personal communication, 2010).

The upwelling events are characterized by strong wind and cooler surface temperatures near shore and on the shelf. There were two general patterns in the

surface water: the upwelling cross-shore or upwelling along-shore. We found in collaboration with the MIT-MSEAS group that the first upwelling event, from August 1 to August 5, was primarily cross-shore. We will focus on this event next in Chapters 3 and 4.

3 Simulations and Sensitivity Studies

We employed a realistic modeling approach to study the upwelling and relaxation events that occurred during MB06. Specifically, we conducted a large set of sensitivity computer simulations using the MIT-MSEAS System. Our approach consisted of turning off or on a varied set of parameters. By comparing the results of these simulations, we are able to characterize the effects of different factors in these events in the Monterey region. Specifically, the modeling sensitivity studies that we focused on included physical parameters (sub-grid-scale processes), forcing (tides/no tides, specific atmospheric fluxes turned off or on) and numerical and data assimilation parameters (with or without data assimilations, different numerical filters, etc). These modeling sensitivity simulations can provide guidance in subsequent theoretical modeling and help determine which variables need finer tuning.

In what follows, we describe the MSEAS systems and the equations it solves for the physics. We then discuss the different sensitivity simulations that we ran and the model runs.

3.1 MSEAS Primitive Equation Model

The MSEAS system includes a nonlinear free surface primitive equation ocean model with fully implicit 2-way nesting capabilities (Haley and Lermusiaux, 2010); a coastal objective analysis scheme based on fast-marching methods (Argawal and Lermusiaux, 2010); an Optimal Interpolation scheme and Error Subspace Statistical Estimation system (Lermusiaux, 1999; Lermusiaux et al., 2002; Lermusiaux, 2006; Lermusiaux, 2007) for data assimilation, optimization and adaptive sampling; a stochastic representation for sub-grid-scale processes (Lermusiaux, 2006); new schemes for uncertainty predictions based on dynamically-orthogonal equations (Sapsis and Lermusiaux, 2009); nested tidal inversion schemes (Logutov and Lermusiaux, 2008); multiple biological models (Tian et al., 2004); and, several acoustic models (Lermusiaux and Xu, 2010). We have tested the new MSEAS codes in several regions of the world's ocean, including the middle Atlantic Bight, the California coast around Monterey Bay, the Philippine archipelago and the Taiwan-Kuroshio region of the eastern Pacific.

The equations of motion are the primitive equations, derived from the Navier-Stokes equations under the hydrostatic and Boussinesq approximations (Haley and Lermusiaux, 2010; Cushman-Roisin and Beckers, 2010; Lermusiaux and Xu, 2010). Under these assumptions, the state variables are the horizontal and vertical components of velocity, (u,w), the temperature, T , the salinity, S and the surface elevation, η. Denoting the spatial positions as (x, y, z) and the temporal coordinate with t, the primitive equations can be written as:

Conservation of Mass

$$\nabla \bullet \vec{u} + \frac{\partial w}{\partial z} = 0 \tag{3-1}$$

Conservation of Horizontal Momentum

$$\frac{D\vec{u}}{Dt} + f\hat{k} \times \vec{u} = -\frac{1}{\rho_0}\nabla p + \vec{F} \tag{3-2}$$

Conservation of Vertical Momentum

$$\frac{\partial p}{\partial z} = -\rho g \tag{3-3}$$

Surface Elevation

$$\frac{\partial \eta}{\partial t} + \nabla \bullet (\int_{-H}^{\eta} \vec{u} dz) = 0 \tag{3-4}$$

Conservation of Internal Energy

$$\frac{DT}{Dt} = F^T \tag{3-5}$$

Conservation of Salt

$$\frac{DS}{Dt} = F^S \tag{3-6}$$

Equation of State

$$\rho = \rho(z, T, S) \tag{3-7}$$

where p is the pressure, f is the Coriolis parameter, ρ is the density, ρ_0 is the (constant) density from a reference state, g is the acceleration due to gravity, H is the water depth in the static ocean and $\hat{k}$ is the unit direction vector in the vertical direction. The turbulent sub-gridscale processes are represented by $\vec{F}$, F^T and F^S.

3.2 Sensitivity Studies

The primitive-equation model was run with 2-way nesting and grid computing capability. The domains were as described in Section 2.3.2, but the model numerics were improved to allow 2-way nesting with a free-surface. The baseline simulation was forced with everything on. Atmospheric fluxes (wind, evaporation minus precipitation, radiation, and heat fluxes) were imposed at the surface. Data was assimilated twice daily and the model was further forced with barotropic tides at lateral boundaries with a mixed open boundary condition scheme. The baseline run started on July 27th and ran through August.

Upwelling is a complex phenomenon, and we wanted to study the effects of various forcings and data assimilation in the simulated dynamics to understand it better. We varied the surface forcings (wind, heat, evaporation minus precipitation (EMP), and radiation), as well as the length of time that data was assimilated and whether or not tidal forcing was included. Table 1 summarizes these model runs.

Table 3-1: Run Chart. "1" means the value was set to "on," "0" means the value was set to "off," and " 2" means the value was "on" until August 1 (the start of the first upwelling event, 5 days after the start of the run) and then turned to "off." The runs in bold will be examined in more detail in this chapter

Run Number	Atmospheric Forcings				Data Assimilation	Tides
	Wind	Heat	EMP	Radiation		
1	**1**	**1**	**1**	**1**	**1**	**1**
2	**1**	**0**	**0**	**0**	**1**	**1**
3	**0**	**1**	**0**	**1**	**1**	**1**
4	0	0	1	0	1	1
5	0	0	0	1	1	1
6	**0**	**0**	**0**	**0**	**1**	**1**
7	1	1	1	1	0	1
8	**1**	**1**	**1**	**1**	**2**	**1**
9	0	0	0	0	0	1
10	1	1	1	1	1	0
11	1	1	1	1	1	2
12	1	1	1	1	0	0
13	1	1	1	1	2	2

For each run, we examined the temperature at depths of 0m (surface), 30m (thermocline), 150m (below the thermocline and near the expected undercurrent).

The rest of this section focuses on a few key runs: run 1 (baseline), run (2) with only wind surface forcing and data assimilation and tides throughout, run (3) with only heat surface forcing and data assimilation and tides throughout, run (6) with no

surface forcings and no data assimilation, and run (8) with data assimilation until the start of the first event. These are the runs that show the most variation or that are expected to be most important in explaining upwelling dynamics and its simulations. We focus on the first upwelling event.

3.2.1 Baseline (Run 1)

In the baseline run, all forcings were used, data was assimilated, and tidal forcings were included. Figure 3-1 shows the surface temperature in this run during the first upwelling event.

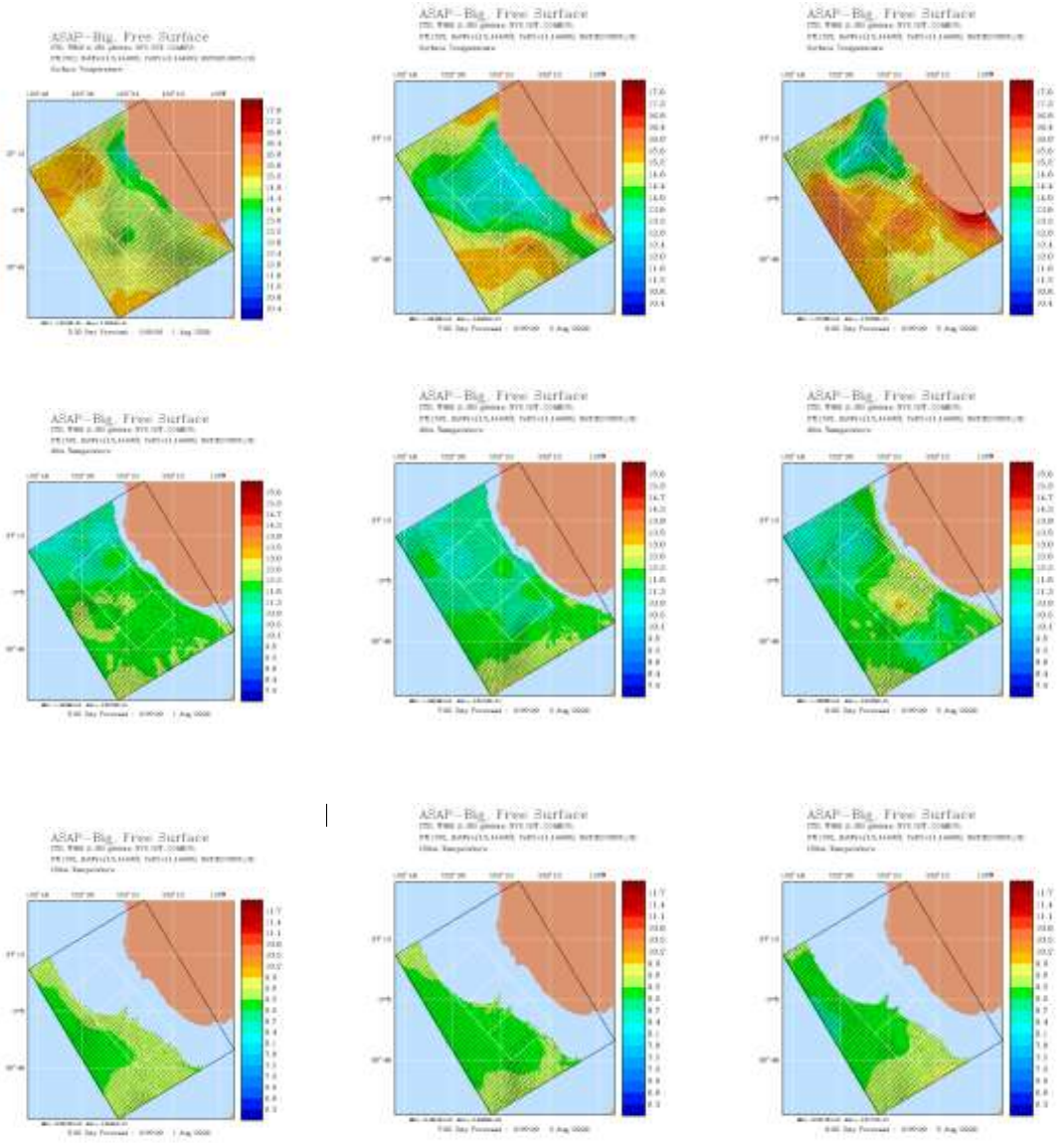

Figure 3-1: Temperature at 0, 30, and 150 meters deep on August 1 00Z, August 3 00Z, and August 5 00Z, 2006 for a baseline MSEAS primitive-equations simulation.

The leftmost column on Fig 3-1 is temperature fields at 0m, 30m and 150m, on August 1st at 00Z, which is at the start of the event when the surface is still warmer but some upwelling is starting along the coast. The middle column is fields on August 3rd 00Z which corresponds to the middle of the event when cold water has upwelled to the surface. The rightmost column of Fig 3-1 is fields on August 5th 00Z which is at the end of the event when the surface starts warming again. Even though the wind acts at the surface, the deeper fields show the effects of upwelling by conservation of mass and wind mixing. For example, at 30m depth, one can definitely see the cooling in the middle of the event and the start of the relaxation on the last day (Aug 5), with warming along the coast due to mixing and warming in the shallower portions of the Ano Nuevo shelf. Finally, note the relation to these plots and the wind direction in Fig 2-5; the upwelling event occurs when the wind is strong in the positive direction.

3.2.2 Only Wind surface forcing (Run 2)

Another set of model runs was conducted altering the forcings (Runs 2-6 in Table 3-1). In general, the wind plays an important role in upwelling dynamics, so one would expect the run with wind forcing to resemble closely the full run. However, in the Monterey Bay region, the importance of wind forcing (wind stress curl) relative to heat flux and surface atmospheric pressure effects is still debated in the scientific literature (e.g. Ramp et al., 2009). This was one of the motivations for our realistic modeling sensitivity study.

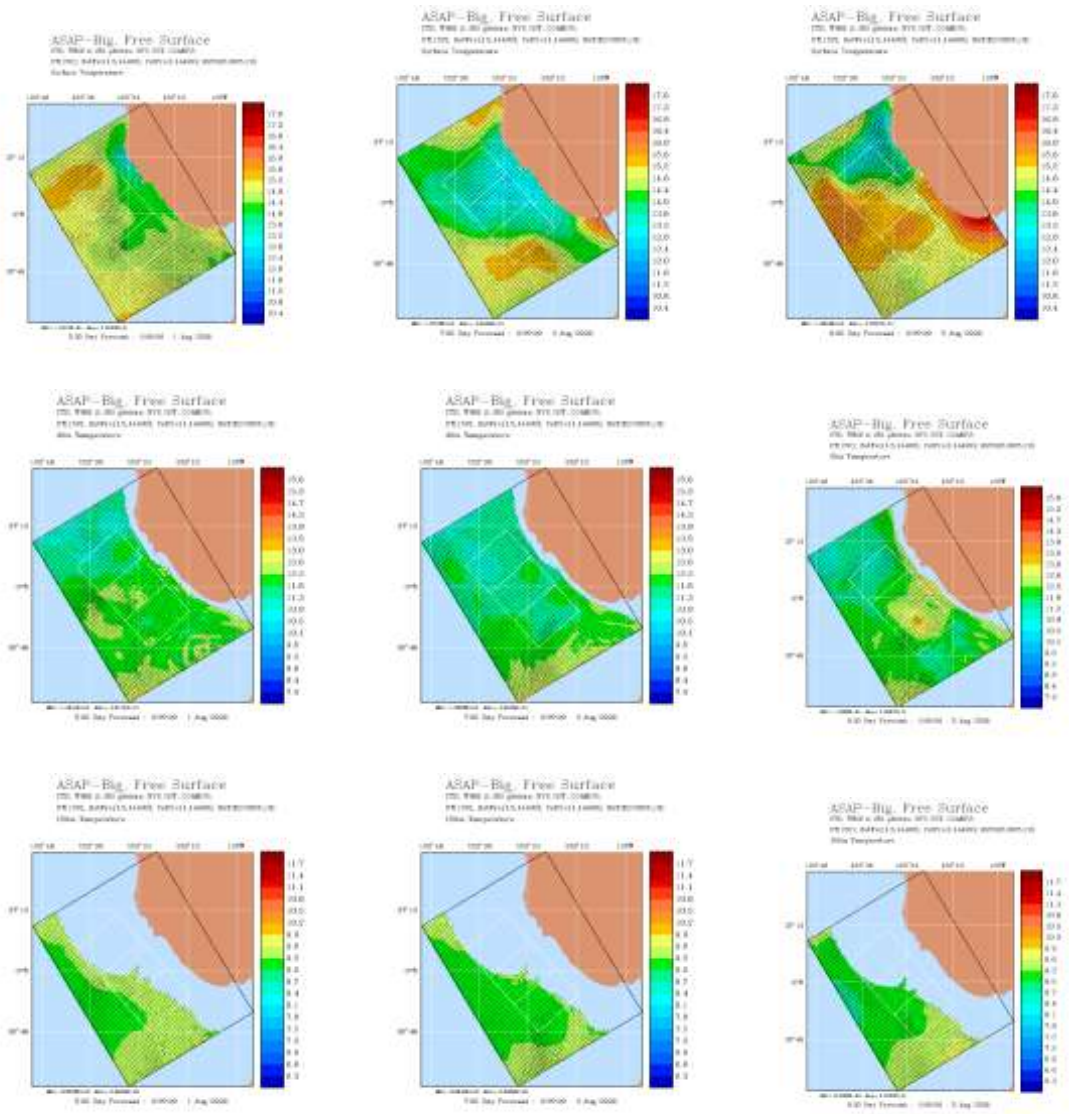

Figure 3-2: Temperature at 0, 30, and 150 meters deep on August 1, August 3, and August 5, 2006 for a MSEAS primitive-equation simulation with only wind surface forcing.

The striking result is that this run, forced only by wind stress at the ocean surface, compares closely to the baseline. Both runs show the same features of roughly the same size in similar locations. These similarities extend to all depths although the images from 30 and 150 meters deep are more similar. This is because atmospheric fluxes have a stronger impact in the surface ocean layers. Overall, these results show that for this first upwelling event at Ano Nuevo (Aug 1-Aug5, 2006), the wind stress is the important driver of the upwelling dynamics.

3.2.3 Only Heat surface forcing (Run 3)

We now examine the results of the run with only heat surface forcing. If we superimpose the results from this run with those of the run with wind forcing only (Sect 3.2.2), we are left with something that very closely resembles the baseline (Sect. 3.2.1). Forcing due to water flux (evaporation minus precipitation) and radiation seem to play a much smaller role (runs not shown). A first result is that when only surface heat fluxes are utilized, the upwelling is much reduced. A second result is that, while there is no wind forcing, we still see evidence of some upwelling. This might be due to the data assimilation.

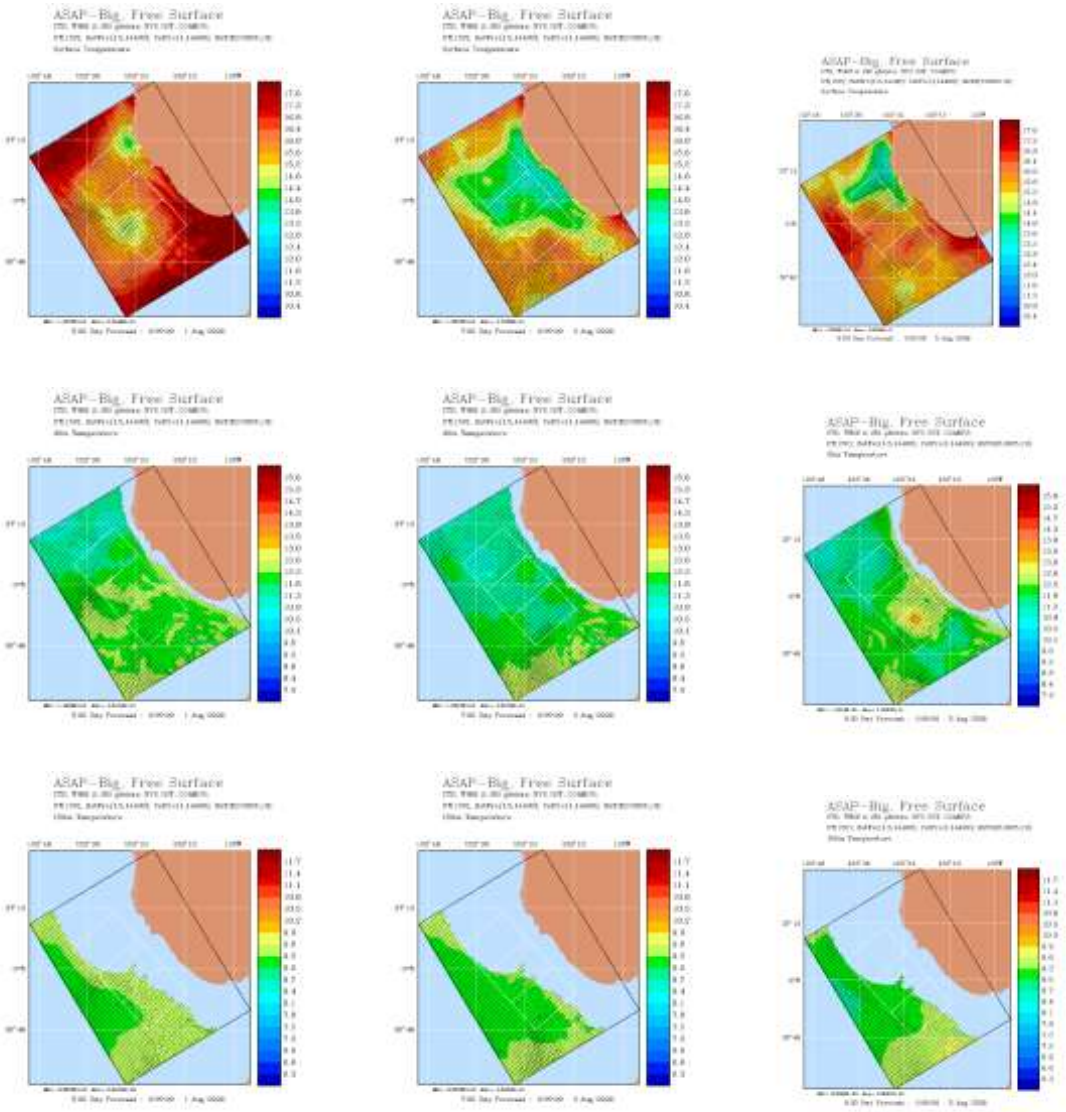

Figure 3-3: Temperature at 0, 30, and 150 meters deep on August 1, August 3, and August 5, 2006 for a MSEAS primitive-equation simulation with only heat surface forcing.

At the surface, the values from this run are much warmer than those of the baseline, especially on August 1. However, both sets of figures show some similar features in similar locations. At 30m and 150m deep, the values and features are much closer to those of the baseline. This is expected since we are only varying surface forcing. However, differences are present at 30m; the temperatures are overall warmer and less uniform in space at locations where upwelling would act by conservation of mass (see Sect 2.1) and mixing. This patchier field could be due to data assimilation. The assimilated data could bring in upwelled waters where upwelling happened but not elsewhere where simulations without wind stress forcing could not have been able to simulate the upwelling (if wind stress is the main upwelling control). To answer these sorts of questions, we also tested several simulations with no data assimilation at all as well as simulations with data assimilation only to the beginning of the event (see Sect 3.2.5).

3.2.4 No Surface Forcing (Run 6)

Next we examine the run with no surface forcing to see whether the upwelling we see in figure 3-3 is a result of the data assimilation or is driven by some other factor. The result is that we see the same kind of upwelling spots as the run with only surface heat fluxes (Sect 3.2.3), which leads us to conclude that the upwelling that is not wind-driven is an artifact of data assimilation and not one of the other forcings. The difference between this run and run 3 is the relative magnitude of the upwelling. The surface forcing accentuates the gradients between the regions with upwelling and the regions without, but the shapes of the features remain relatively similar.

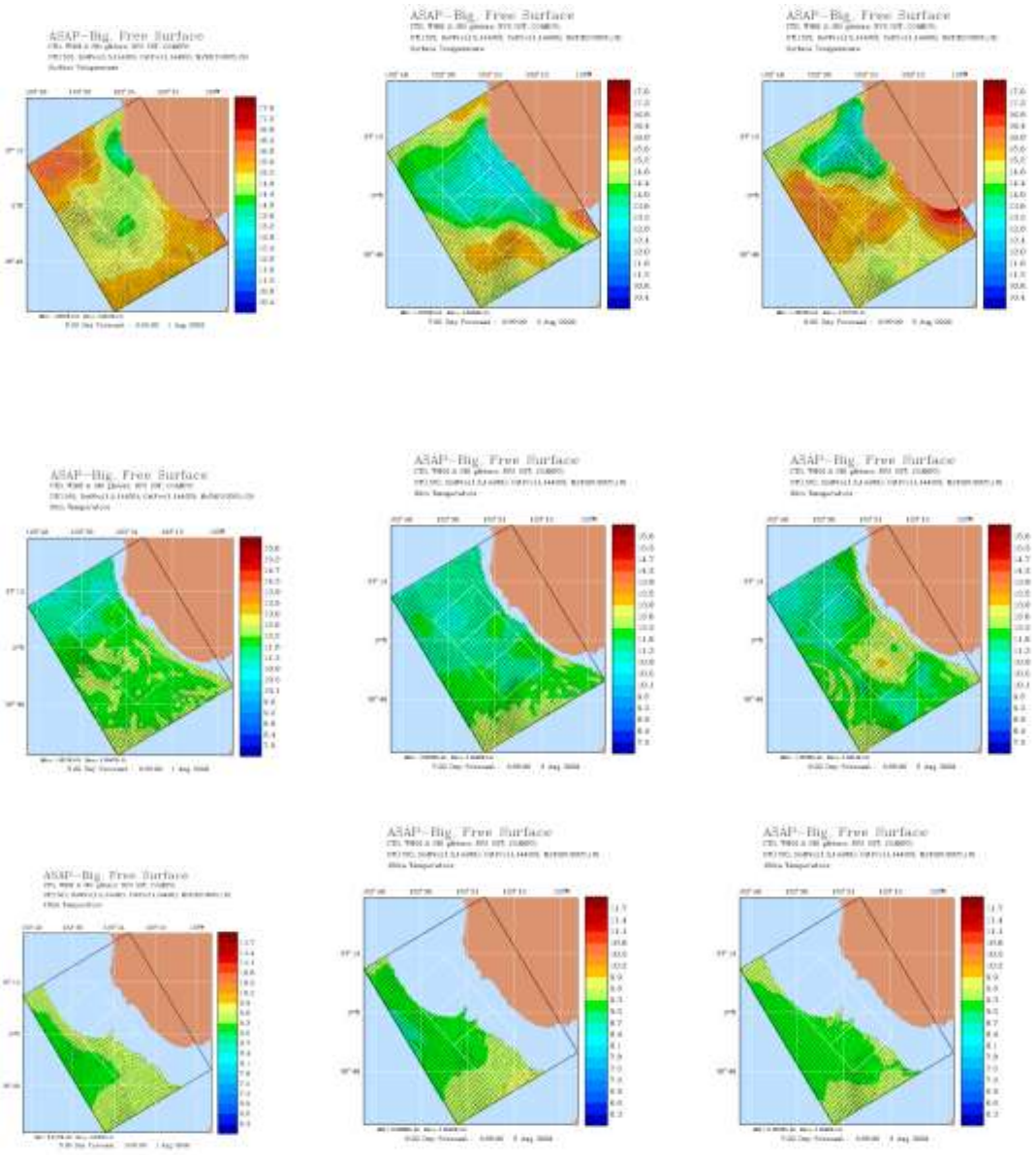

Figure 3-4: Temperature at 0, 30, and 150 meters deep on August 1, August 3, and August 5, 2006 for a MSEAS primitive-equation simulation with no surface forcing.

3.2.5 No Data Assimilation after start of first event (Run 8)

The baseline results (Figure 3-1) can be compared to those for the run without data assimilation, Figure 3-6, to examine the effects of data assimilation. The data is assimilated up to the start of the first event (August 1 0:00:00) so that the conditions at the start of the two runs are identical. Data is not assimilated after the start of the event so the differences between the two runs become more noticeable as more time elapses. This confirms Lorenz's work on predictability limits; lacking any external information such as that gained from data assimilation, small uncertainties will grow larger until the forecast is no better than one drawn randomly (Lermusiaux, 2006; DelSole and Tippett, 2007).

In our particular case, data assimilation effects arise from within the domain but also from the exterior of the domain through the boundary conditions. In the baseline run, data is assimilated in the larger domain and this information flows in the small high-resolution domain (all domains plotted on the Figs. of Sect 3). These inflows of data assimilated outside the small domain are clearly visible at depth in the southern region: they correspond to inflows from the poleward offshore sub-surface currents. They are significant because by August 1, the ships and underwater vehicles are still on their way to sample the large domain for the first time: the initialization survey is not yet complete.

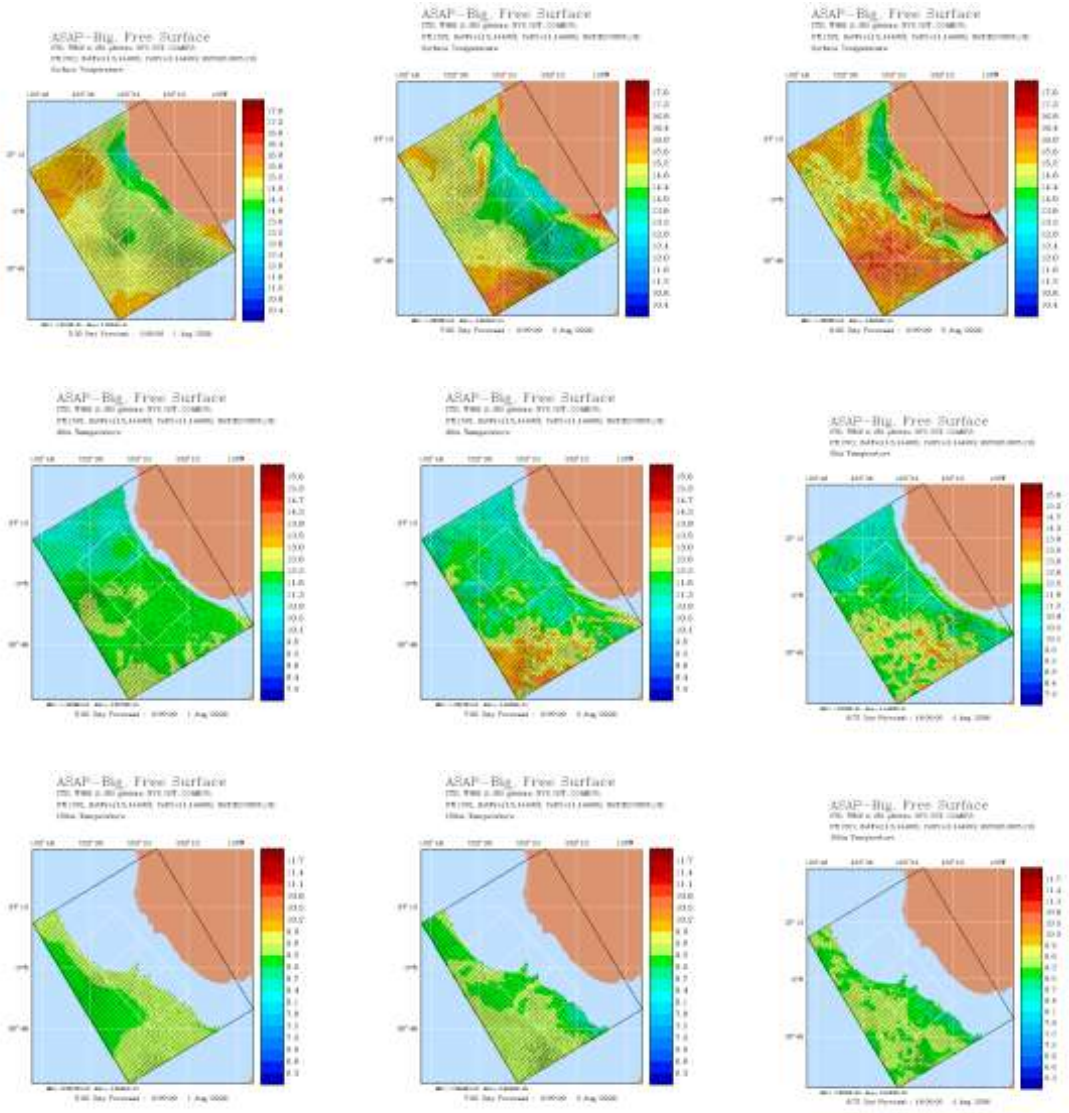

Figure 3-5: Temperature at 0, 30, and 150 meters deep on August 1, August 3, and August 5, 2006 for a MSEAS primitive-equation simulation no data assimilation after July 31.

There is still upwelling, but the shape of the upwelling is different than in Figure 3-4. Nonetheless, on the shelf and in regions with no inflows from the large domain, we still see upwelling occurring at similar locations as in the baseline run. Utilizing the results of the previous runs, we can thus conclude that the first upwelling event is in a large part driven by wind stress forcing, and not by other atmospheric fluxes. We can also conclude that data assimilation (inside the small domain but also most

importantly outside of this domain) plays a role in determining the shape of the upwelling event

3.2.6 Conclusions

In summary, our varied sensitivity simulations show that altering the surface forcings leads to larger differences at the surface than at depths of 30 and 150 meters compared to the baseline. Wind forcing and data assimilation were the two variables examined that had the largest difference on whether there was upwelling and the shape of the upwelling event. Chapter 4 next examines the time-averaged mean heat fluxes and volume-averaged temperature variability for all of the runs for this first upwelling event. This allows us to provide quantitative estimates in the thermal energy and heat flux balances in the region, including their evolution with time during the event.

A second upwelling event occurred between August 9th and August 13th. This upwelling event was characterized by cooler water mostly alongshore.

3.3 Second Upwelling Event

A second upwelling event occurred during MB06 from August 9 00Z to August 13 00Z. Again, this event correlates with strong wind stress in the upwelling favorable direction (refer to Fig 2-5). The signature of this upwelling event is more alongshore than the first upwelling event. This illustrates that upwelling is not simply a 2-D phenomenon that always reproduces itself. First, the wind forcing of the second event is different. Second, the background state does not correspond to a strong northward flow in this second event. Overall, this second upwelling plume is transported southward by the upwelling quasi-geostrophic currents.

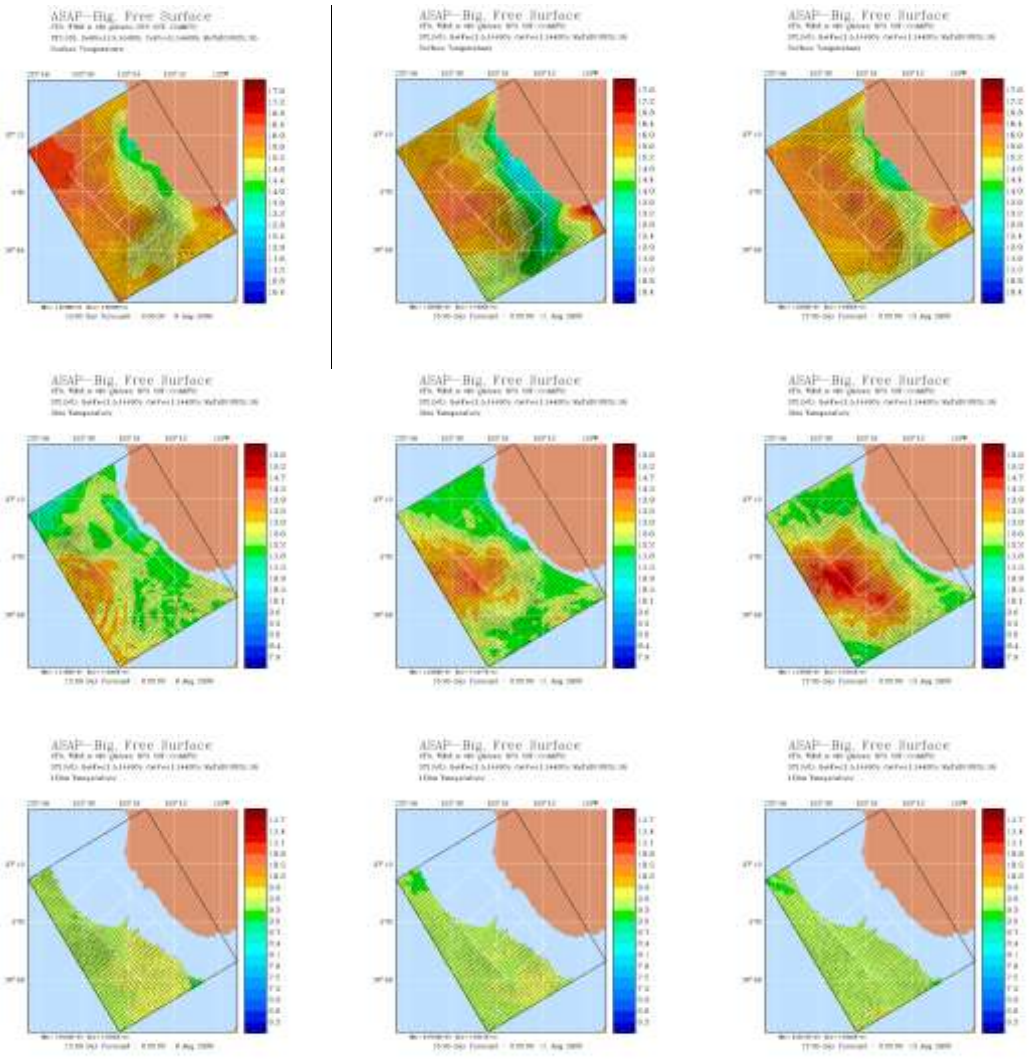

Figure 3-6: Temperature at 0, 30, and 150 meters deep on August 9, August 11, and August 13, 2006 for a baseline MSEAS primitive-equation simulation.

4 Heat Flux and Mean Temperature Variability

Our approach to better understand upwelling and relaxation events in the Monterey Bay region consist of running computer simulations using the 2-way nested primitive-equation model of MSEAS, varying the surface forcings (wind, heat, evaporation minus precipitation (EMP), and radiation), tidal forcing, as well as the length of time that data were assimilated. In addition to describing the results of these simulations (Chap. 3), we quantified the thermal energy balance in the Ano Nuevo region, focusing on the time-averaged heat fluxes over the surface and sides of the small domain, as well as the variability in time of the volume-average temperature field. For these quantifications of thermal energy, we focus again on the first upwelling event, from August 1st to August 5th.

4.1 Thermal Energy Fundamentals

This section first reviews the fundamentals behind our thermal energy balance computations and then explains the software we used to calculate it for each of the runs.

4.1.1 Thermal Energy Balance

To analyze the thermal energy fluxes, we start from the first law of thermodynamics (Cushman-Roisin and Beckers, 2010) applied to a control volume of ocean water:

$$\frac{d}{dt}\int_{CV}\rho(e+\frac{v^2}{2}+gz)dV=\dot{Q}-\dot{W}_{shaft}-\int_{CS}\rho(h+\frac{v^2}{2}+gz)(\vec{v}_r\cdot\vec{n})dA \qquad (4\text{-}1)$$

where t is time, CV is the control volume, ρ is density, e is the internal energy, v is velocity, g is gravity, z is depth, $\dot{Q}$ is the rate of heat added to the system, $\dot{W}_{shaft}$ is the rate of shaft work done by the system, CS is a control surface, h is the enthalpy, $\vec{n}$ is the normal from the control surface.

For an incompressible fluid, the constitutive relation for a change of enthalpy *h* from state 1 to 2 is:

$$h_2 - h_1 = c(T_2 - T_1) + \frac{1}{\rho}(P_2 - P_1) \tag{4-2}$$

where *c* is the heat capacity, *T* is the temperature, and *P* is the pressure.

In this case, with our ocean model's hydrostatic approximation in the vertical, we can assume that at the same depths, the pressures are equal. This allows us to cancel out the pressure terms in the surface integral. If we assume a constant specific heat capacity, c, neglect kinematic and gravitational changes when compared to thermal advective flux changes, neglect variations of density when compared to variations in temperatures (i.e. density then cancels out), and cross out shaft work, then the equation simplifies to:

$$\frac{d}{dt}\int_V T dV = \int_{surface} \vec{q} \cdot d\vec{A} + \int_{north} T\vec{v} \cdot d\vec{A} + \int_{south} T\vec{v} \cdot d\vec{A} + \int_{west} T\vec{v} \cdot d\vec{A} \tag{4-3}$$

Equation 4-3 shows that the thermal energy balance of the volume of interest (a domain around the Ano Nuevo region) has a diffusive flux at the ocean surface and horizontal advective fluxes through each open boundary (North, South, and West sections). We are assuming that there is no heat flux through the ocean floor or the coast (east boundary). The units of the time-rate-of-change of the volume-averaged temperature field in the right hand-side are K m^3/s.
The surface "temperature flux", *q*, is defined as:

$$q = \frac{q_{surface}}{\rho c} \tag{4-4}$$

where $q_{surface}$ is the surface heat flux in W/m^2 . Thus, *q* has units of K m/s.
The units of all temperature fluxes in the left hand side are thus in K m/s.

In Section 4.2, we will look at the heat flux through each of the four surfaces individually and compare each run to the baseline.
Notes: i) the surface heat flux will either be identical to the baseline or be roughly zero depending on whether the surface heat forcing is "on."
ii) in Sections 4.2 and 4.3, the units of the variables that are plotted are for the right-hand-side, K/s (we divide the quantity by the whole volume in section 4.3) while the units of the surface and lateral fluxes (in the left hand-side) plotted in section 4.2 are K cm/s.

4.1.2 Software

The heat fluxes and volume-averaged time rate of change in equation 4-3 were calculated using the MSEAS fields from Chapter 3 and summed through the

boundaries using a Matlab script. This software (Lermusiaux and Haley, personal communication) first reads the ocean fields simulated by the primitive-equation model of MSEAS (see Sect 3.1). The three lateral flux terms in equation 4-3 are computed by integration along the side boundaries, using the MSEAS simulated temperature, salinity and velocity (currents) fields. The surface heat flux term is computed by integration of the local flux boundary condition. The time rate of change term on the left hand side is computed by integration over the volume at two different times. It is also computed by a simple sum of the four flux terms on the right hand side. The software can compute such flux balances on any volume of ocean chosen by the user. MSEAS fields are first interpolated onto the chosen control surfaces and then integrated.

4.2 Mean Fluxes at the Control Volume Surfaces

We utilized the balance equations and software described in Sect 4.1 on the domain illustrated on Figure 4-1. This control volume focuses on the shelf at Ano Nuevo where the upwelling is often the strongest.

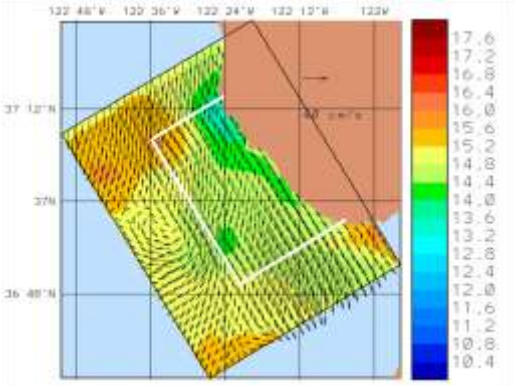

Figure 4-1: The white box outlines the domain (control volume) used for calculating time-averaged lateral and surface fluxes, and volume-averaged time rate of change of temperature.

We computed each terms in equation 4-3 for a large set of simulations, including those listed in Table 3-1. In what follows, we present the results for the baseline (Sect 4.2.1), only-wind-forcing (Sect 4.2.2), only-heat-forcing (Sect 4.2.3), only-evaporation minus precipitation (emp)-forcing (Sect 4.2.4), only-radiation-forcing (Sect 4.2.5), no surface forcings (Sect 4.2.6), all forcings but no data assimilation (Sect 4.2.7), no data assimilation after the start of the first event (Sect 4.2.8), no surface forcings and no data assimilation (Sect 4.2.9), all surface forcings and data assimilation but no tidal forcing (Sect 4.2.10), no tides after the start of the first event (Sect 4.2.11), no data assimilation and no tides (Sect. 4.2.12), and no data assimilation after the start of the first event and no tidal forcing after the start of the first event (Sect 4.2.13).

4.2.1 Baseline (Run 1)

For each figure, a few key features were identified. On the Northern section (upper right), the key features are: (a) the location with negative flux (equatorward) near the surface, and (b) the location with positive flux (poleward) near the coast on the shelf. For the Southern section (lower right), the key features are: (c) the location with positive heat flux (poleward) on the Ano Nuevo shelf, (d) the deeper location with negative heat flux (subsurface cyclonic feature), and (e) the surface signature of the upwelling, i.e. the location with negative heat flux near the surface offshore. For the Western section (lower left), the key features are: (f) the location with positive heat flux on the shelf at depth, with a maximum around 20-30m depths, (g) the location with positive heat flux near the surface away from the shelf, (h) the deep location with negative heat flux which correspond to an upwelling jet if such outflows from the shelf southwestward, and i) the surface signature of the upwelling on the shelf in this Western section. If the upwelling was 2D and would reach this offshore Western section, the upwelling-driven fluxes (f) and (i) would balance each other by conservation of mass: the surface flux (i) is out and the flux f) at depth is in. The Surface (top left) will not be examined in detail since it matches the baseline (equal to the boundary condition heat flux imposed by the atmospheric forcing) or be zero for each of the runs (runs with surface heat flux set to zero).

In what follows, to facilitate the description, we refer to the features by their letter number, from a) to i).

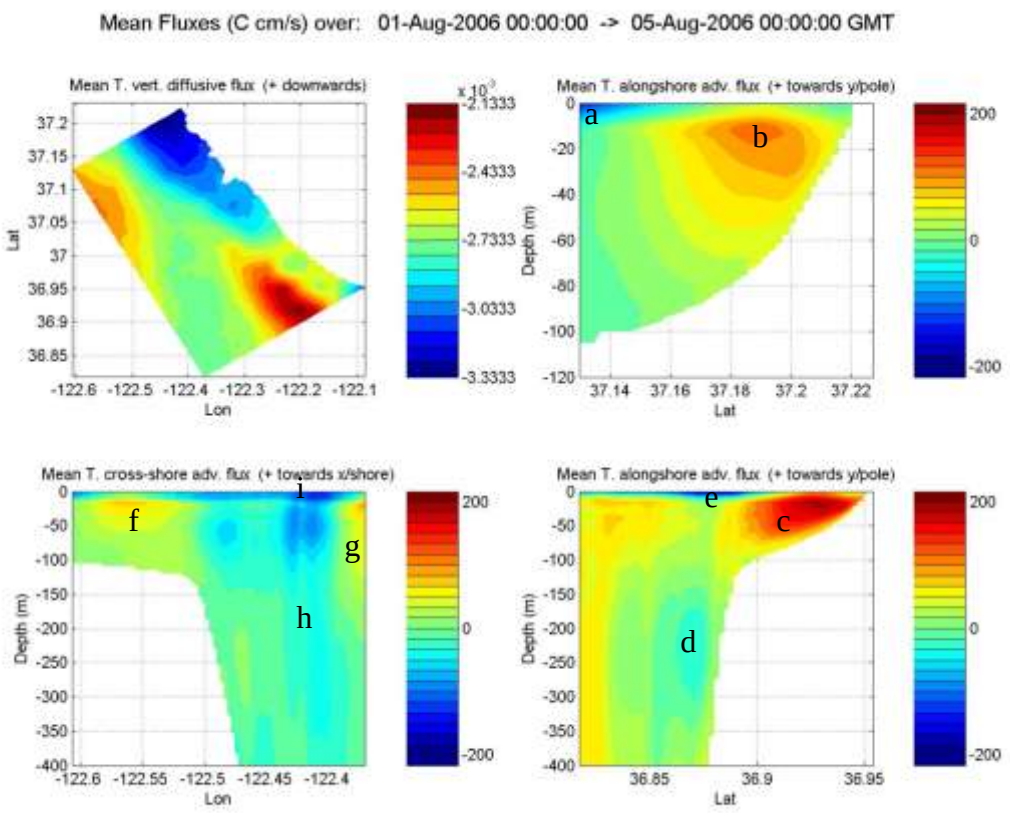

Figure 4-2: Heat Flux (C cm/s) through Surface, the North, South, and West Sections starting in Upper Left and going Clockwise for Run 1.

4.2.2 Only Wind Surface Forcing (Run 2)

The "only wind surface forcing run" (Run 2) has features very similar to the baseline. Feature (a) extends slightly deeper in this run compared to the baseline (this is due to the lack of heat forcing in Run 2). The magnitude of the flux at point (d) is also slightly higher, although the shape is identical. Feature (g) extends slightly deeper on this run, and the heat flux at point (h) is slightly less. Importantly, the features a), b), e), f) and i), which are characteristic of the upwelling, are very close to the baseline. Overall, the thermal energy balance of the run with only wind forcing is thus very similar to the baseline. This strengthens the hypothesis that the wind stress plays a dominant role in this first upwelling event in the Monterey Bay region.

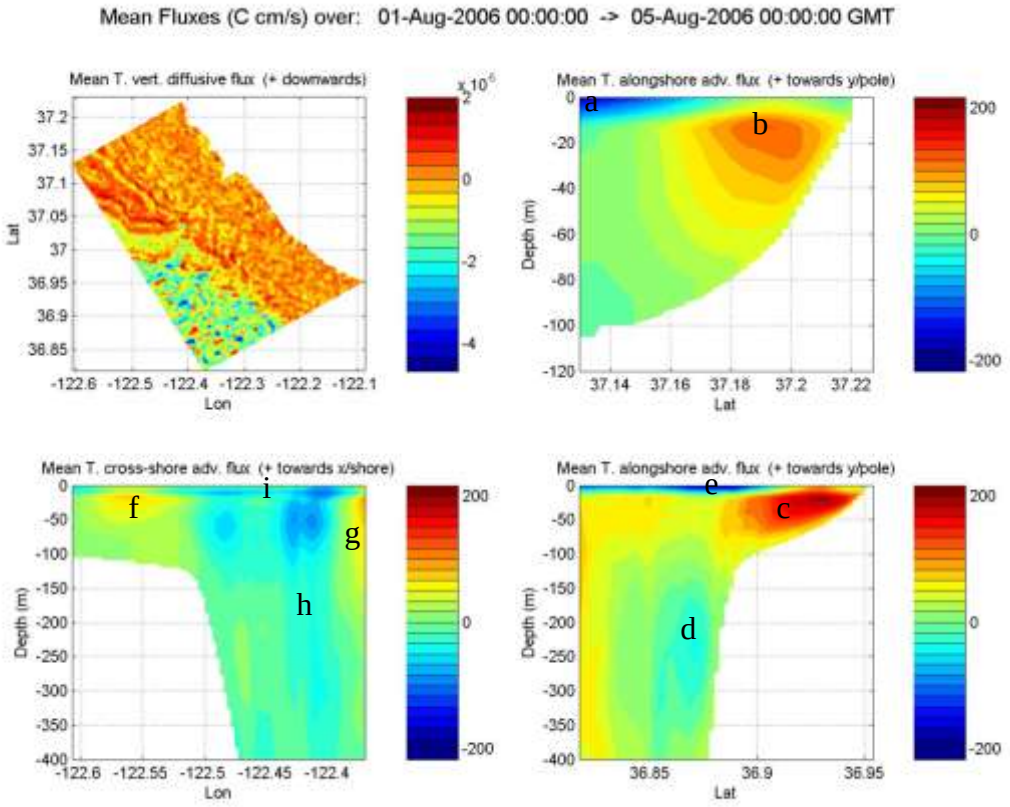

Figure 4-3: Heat Flux (C cm/s) through the Surface, North, South, and West Sections starting in Upper Left and going Clockwise for Run 2.

4.2.3 Only Heat Surface Forcing (Run 3)

Features (a), (e) and (i) which represent the upwelled waters advected offshore are missing entirely from the run with only surface heat flux forcing; there are no negative (offshore) heat fluxes in the surface layers. Feature (b) is significantly larger; it starts at the surface and extends deeper. This indicates that the northward flow observed on the shelf during this period is substantially reduced when upwelling favorable winds occur. Feature (c) extends slightly deeper and is longer, but the maximum value of the heat flux is the same in both this run and the baseline. Feature (d) has a similar shape but its value is less than in the baseline. Feature (f) is closer to the surface and is smaller (which is normal, as this would be the response to upwelling at depth, in the form of a flux towards the shore, but it is not present when wind stresses are not applied at the ocean surface). Feature (g) has a slightly higher value and starts at the surface as opposed to about 10 meters below the surface.

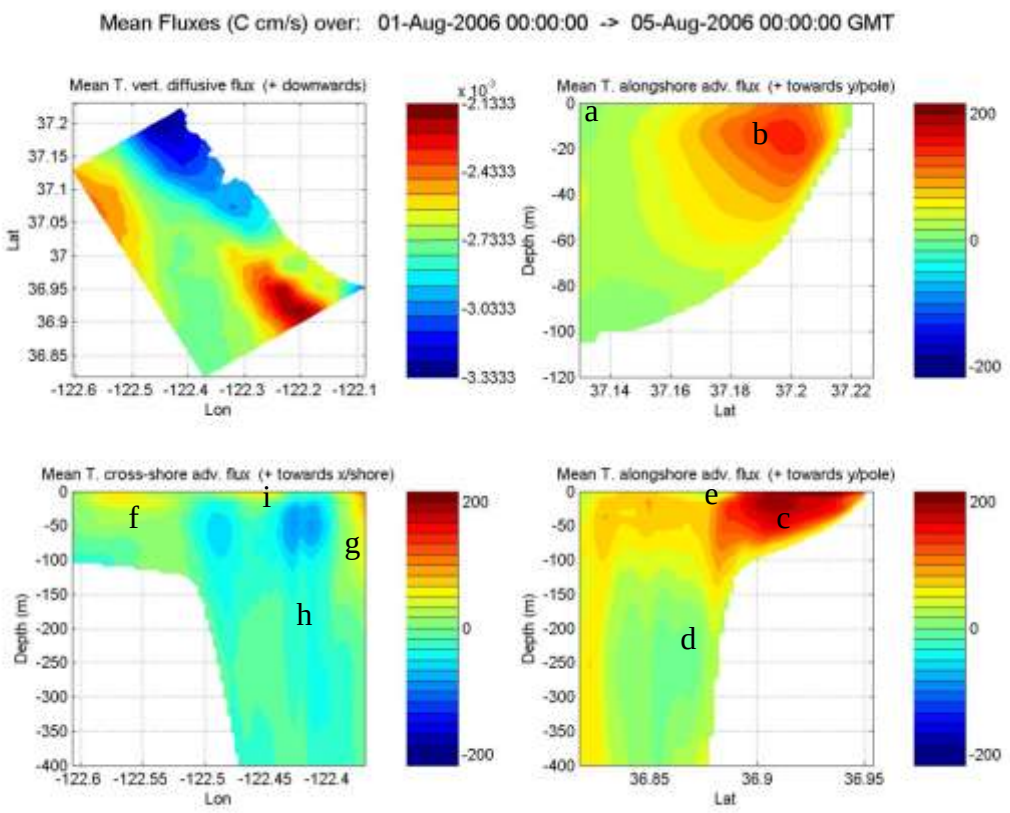

Figure 4-4: Heat Flux (C cm/s) through the Surface, North, South, and West Sections starting in Upper Left and going Clockwise for Run 3.

All of the features that were present in the baseline are present in this run except for features (a) (e), (i) and (f). We can now conclude that those features are a result of the wind surface forcing, while the mean northward flows (b) and (c) are stronger when upwelling is not present

4.2.4 Only Evaporation Minus Precipitation (EMP) Surface Forcing (Run 4)

The Run with "Only Evaporation Minus Precipitation (EMP) Surface Forcing" (Run 4) closely resembles Run 3 ("Only Heat Forcing").

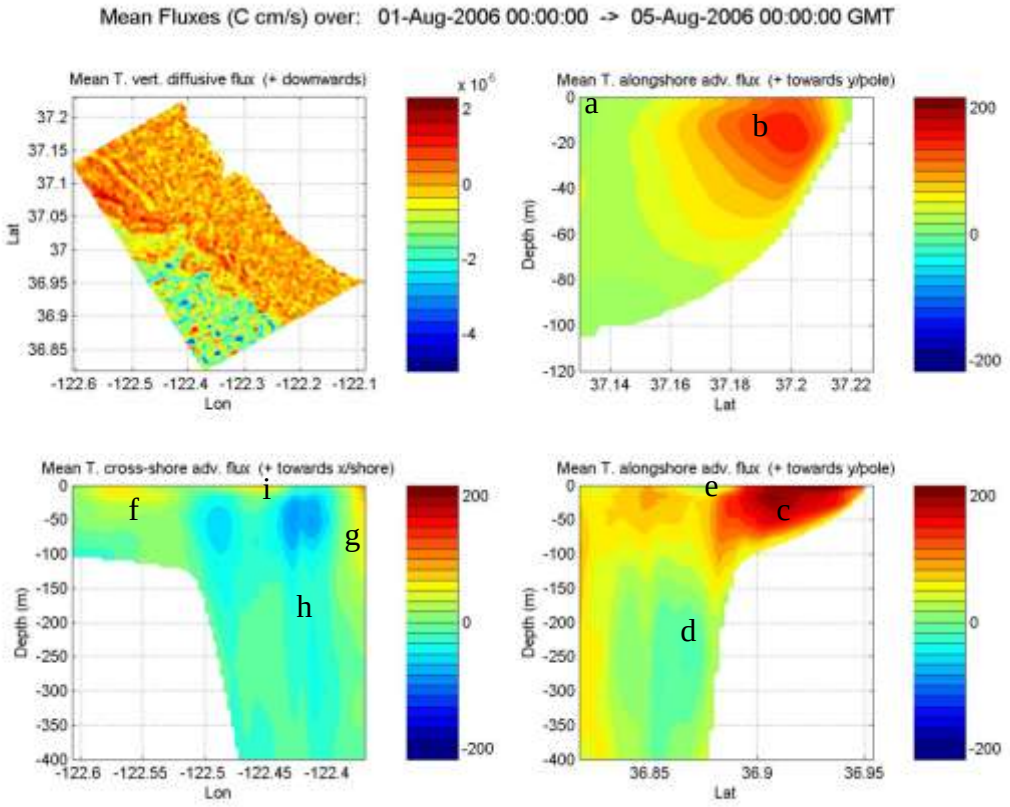

Figure 4-5: Heat Flux (C cm/s) through the Surface, North, South, and West Sections starting in Upper Left and going Clockwise for Run 4.

That this run is missing features (a), (e) (i) and (f) tell us that the evaporation minus precipitation forcing is not involved in the upwelling.

4.2.5 Only Radiation Surface Forcing (Run 5)

The run with only radiation surface forcing (Run 5) also resembles Runs 3 and 4, those with only surface heating forcing and evaporation minus precipitation forcing, more than it resembles the baseline (Run 1).

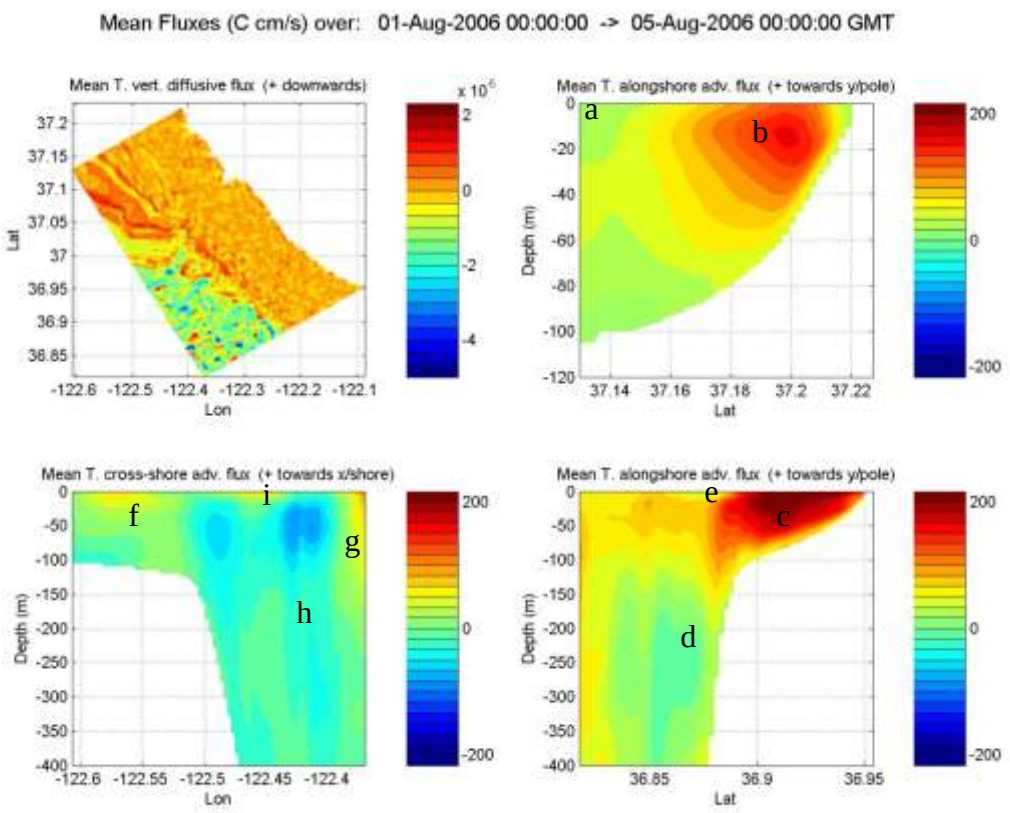

Figure 4-6: Heat Flux (C cm/s) through the Surface, North, South, and West Sections starting in Upper Left and going Clockwise for Run 5.

Again there is no upwelling driven fluxes corresponding to features (a), (e), (i) and (f); those were only significant when wind forcing was imposed at the surface. However, all of the other features are still present, again with northward flows (c) and (b) much stronger.

4.2.6 No Surface Forcing (Run 6)

The run with no surface forcing (Run 6) also resembles the runs without heat, evaporation minus precipitation, and radiation forcing. This shows that these forcings do not add anything significant to the upwelling dynamics, nor at depth for that matter: it is the upwelling that reduces the northward (poleward) flow at depth on the shelf.

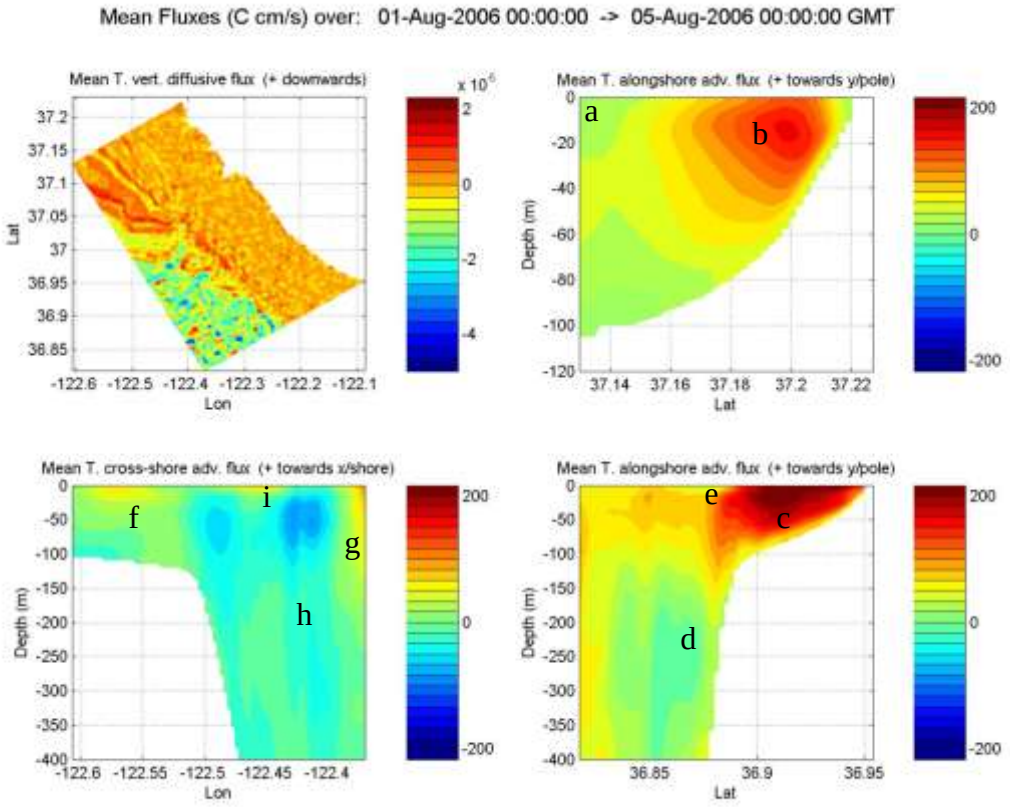

Figure 4-7: Heat Flux (C cm/s) through the Surface, North, South, and West Sections starting in Upper Left and going Clockwise for Run 6.

4.2.7 No Data Assimilation (Run 7)

The run with no data assimilation at all (only data used in the initial conditions on July 27th) but all four surface forcings is distinctly different from any of the runs previously discussed. Feature (a) is similar to that found in the baseline. In feature (b), the area with the highest heat flux extends much deeper and is longer. Feature (c) extends farther offshore and much deeper; it runs into feature (d). Feature (e) is similar to that of the baseline. Feature (f) is further north. Feature (g) is higher in magnitude and covers more area. Feature (h) has a higher magnitude; the area of negative heat flux covers a larger area and is much deeper. Feature (i) which corresponds to the upwelling is also similar, but stronger and its largest amplitudes are a bit further to the north.

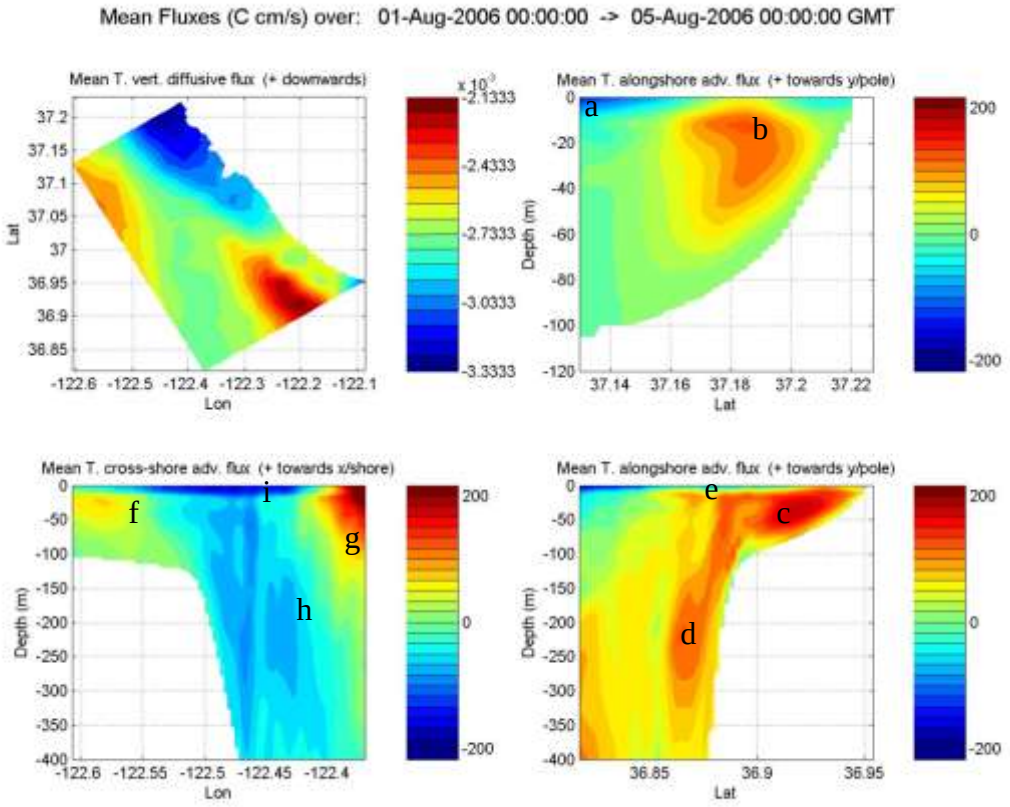

Figure 4-8: Heat Flux (C cm/s) through the Surface, North, South, and West Sections starting in Upper Left and going Clockwise for Run 7.

Features (a), (e), (i) and (f) are present with the wind forcing on. Some of the other features are present but are distorted. Feature (d) is especially different. This figure shows that the data assimilation plays an important role setting the shape of the background features. Without any data, simulations run for a week cannot determine the proper features at depth. This is because what is advected in the region has not felt any synoptic data impact and it is thus basically mean fields from the initial conditions. Sub-surface ocean time scales are much too long to feel the impact of realistic winds over a week or so, and thus an ocean model cannot correct such features without data assimilation.

4.2.8 No Data Assimilation After The Start of First Event (Run 8)

The heat flux plots for the run with no data assimilation after the start of the first event are closer to the baseline than those for the run with no data assimilation at all; however, there are still marked differences. As mentioned in Chapter 3, this is because by the time the first event starts, the sampling has not yet covered enough of the modeling domain; we are still in the initialization phase. Feature (a) has a

higher magnitude and extends deeper. Feature (b) is larger in this run and has a higher magnitude. Feature (c) extends slightly deeper but has the same magnitude. Whereas the heat flux at (d) is roughly zero in the baseline (very weak cyclonic eddy circulation at depth), in this case it has a positive value especially deeper (about 250-400 m). Feature (e) extends deeper than in any other run. Feature (f) also extends deeper than in the others. Feature (i) is much closer to the baseline than in the run with no data assimilation at all. Feature (g) is slightly weaker and does not have the same shape as is seen in the other runs; it is more cross-shore and is less deep. Feature (h) is more similar to the baseline (run 1) than to the run with no data assimilation (Run 7), although the magnitude of the heat flux toward the surface is smaller and is greater deeper compared to the baseline.

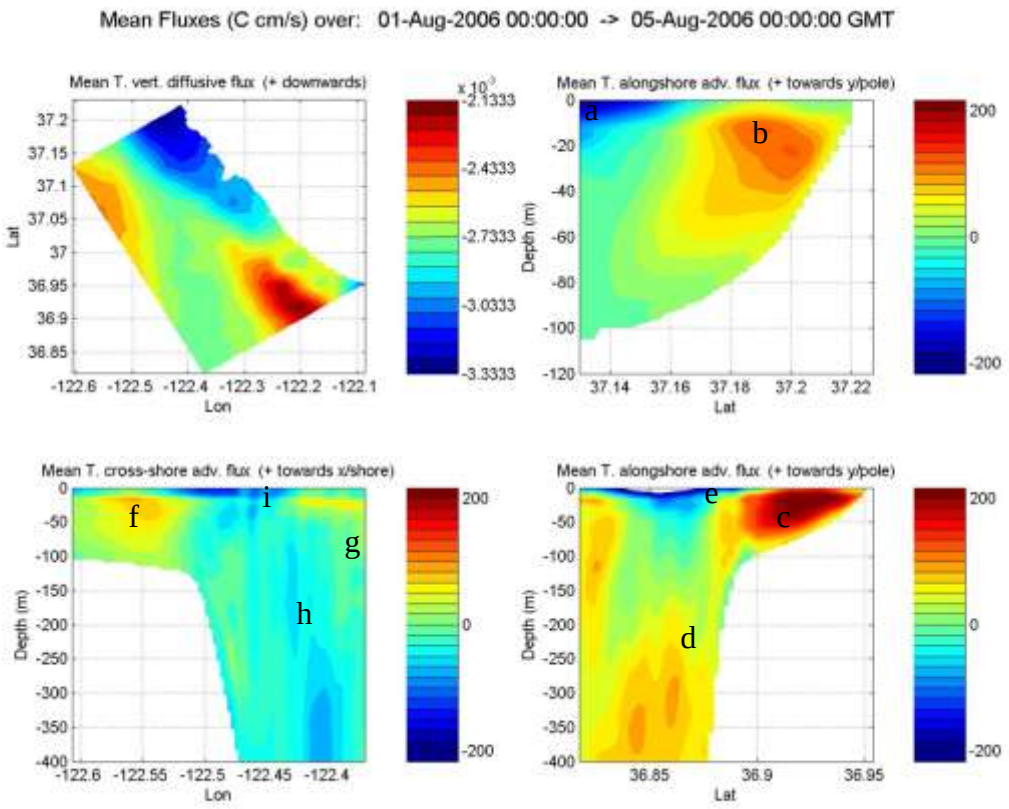

Figure 4-9: Heat Flux (C cm/s) through the Surface, North, South, and West Sections starting in Upper Left and going Clockwise for Run 8.

As expected, this figure looks like a cross between the baseline (run 1) and the run with no data assimilation (run 8) since data was assimilated for the first five days of the run before being turned "off." This shows that for accurate short (1 week or so) predictions, data assimilation is required. Without synoptic data, atmospheric forcing cannot correct the fields at depth.

4.2.9 No Surface Forcing, No Data Assimilation (Run 9)

The run with no surface forcing and no data assimilation at all is very different from the baseline, as expected. Feature (a) and (i) are missing entirely; Feature (b) takes up almost the entire area (the shelf dynamics is fully poleward flow). The magnitude of this poleward heat flux is the same as the baseline, but it starts at the surface and extends farther offshore. This is similar to the run with no surface forcing but it extends even further. Its southern signature, feature (c), is still present and also larger; it extends deeper and more offshore. It is similar to the run with no data assimilation in that the feature extends to the bottom of the domain (400 m). In this case, feature (d) is not present as the positive heat flux extends down the shelf, similar to Run 7. Feature (e) is also absent, similar to Run 6. Feature (f) is missing, although it can be found in Runs 6 and 7. Feature (g) has a higher magnitude, and covers a larger area, both cross-shore and in depth. It starts at the surface, similar to Run 7. Feature (h) also resembles Run 7 in that the magnitude is larger than the baseline and covers a large area, although it does not extend to the coast as it does in Run 7.

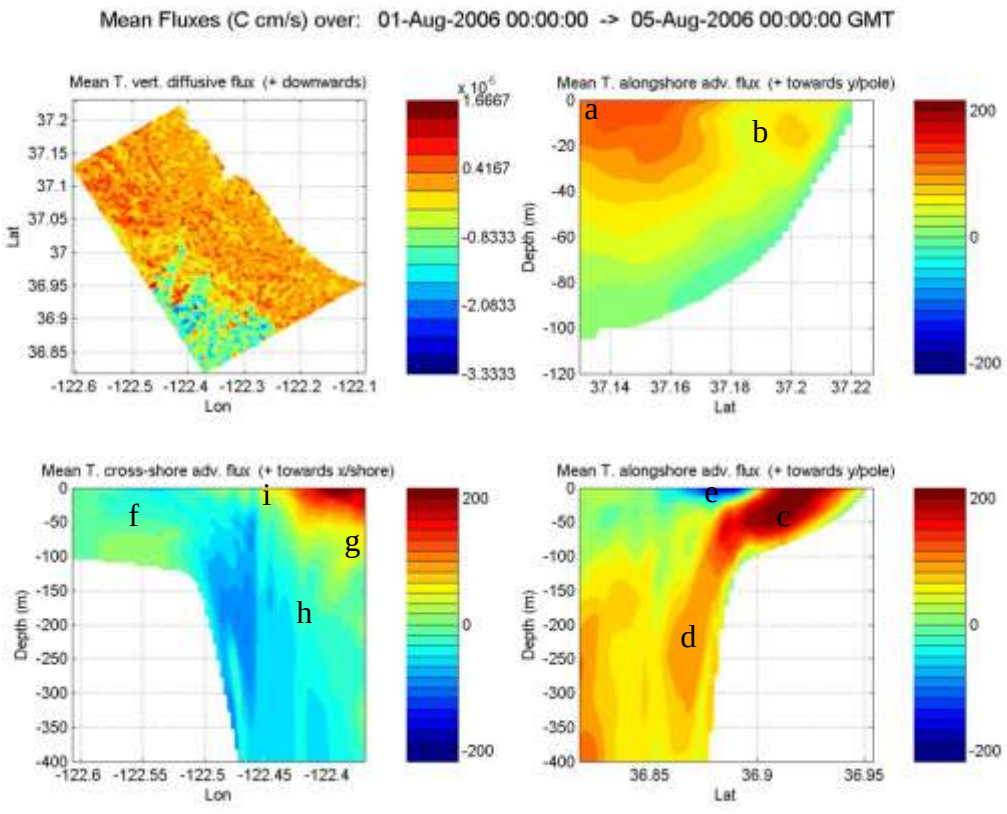

Figure 4-10: Heat Flux (C cm/s) through the Surface, North, South, and West Sections starting in Upper Left and going Clockwise for Run 9.

This run is very different from the baseline; while some of the features are still roughly present (features e, c, and g), they are not very similar. This run does have tidal forcing; however, that is clearly not enough to ensure that the run resembles the baseline. Surface forcings and data assimilation are important control factors.

4.2.10 No Tidal Forcing (Run 10)

This run had no tidal forcing but it does have all four surface forcings and data assimilated in the same way and at the same frequency as the baseline. The features overall are very similar to those of the baseline. One difference is that the flux away from the shore in the southern segment has a slightly smaller value. Feature (c) also extends marginally deeper. Features (f) and (g) also extend deeper. The magnitude of the flux at (h) is smaller. Overall, the differences are not significant. This shows that the tidal forcing is neither a key parameter in generating upwelling, or in generating subsurface flows and features.

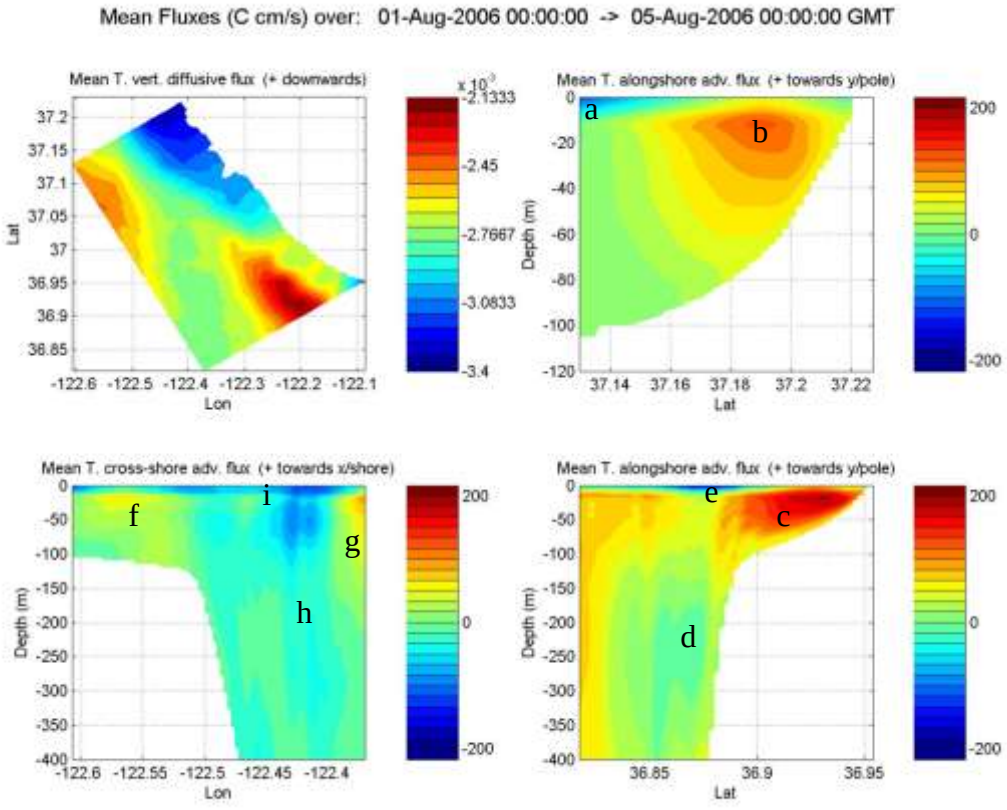

Figure 4-11: Heat Flux (C cm/s) through the Surface, North, South, and West Sections starting in Upper Left and going Clockwise for Run 10.

Again, here we see features (a), (e), (i) and (f) when the wind forcing is included. The features are very similar to the baseline; not having tidal forcing does not seem to be an important for the mean upwelling dynamics.

4.2.11 No Tidal Forcing After Start of First Event (Run 11)

Since the run with no tidal forcing at all did not lead to significant changes in the heat fluxes, we expect that the run with no tidal forcing at the start of the first event will also not have large differences with the baseline. The only difference from the baseline is that feature (f) is smaller in magnitude. All of the other features match the baseline run. This confirms the theory that tidal forcing is not a dominant factor in calculating the mean flux.

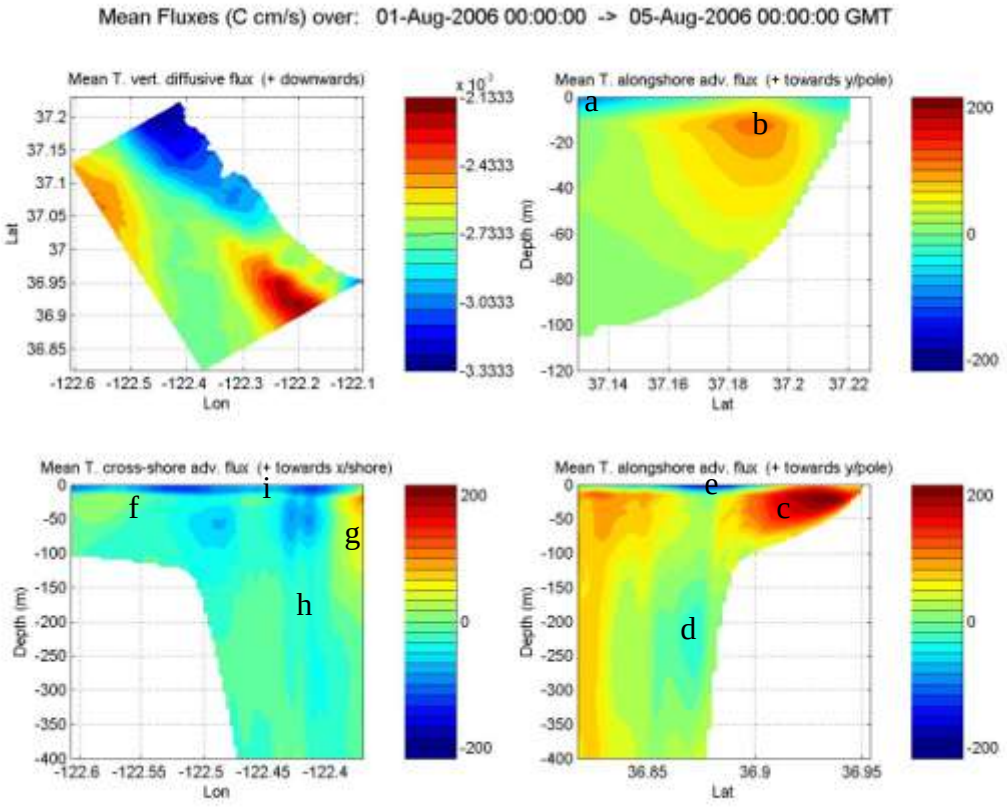

Figure 4-12: Heat Flux (C cm/s) through the Surface, North, South, and West Sections starting in Upper Left and going Clockwise for Run 11.

4.2.12 No Data Assimilation, No Tides (Run 12)

We have already established that tidal forcing is not a significant factor but data assimilation is important. The heat flux for the run with no data assimilation and no tidal forcing should therefore resemble the run with no data assimilation (Run 7). Feature (b) is deeper in Run 12 than the baseline, similar to Run 7, although the maximum flux is not as pronounced as it is in Run 7. The Southern section is also closer to the run with no data assimilation than the run with no tides or the baseline. Feature (g) matches the run with no data assimilation in magnitude but does not extend with its maximum value as deep.

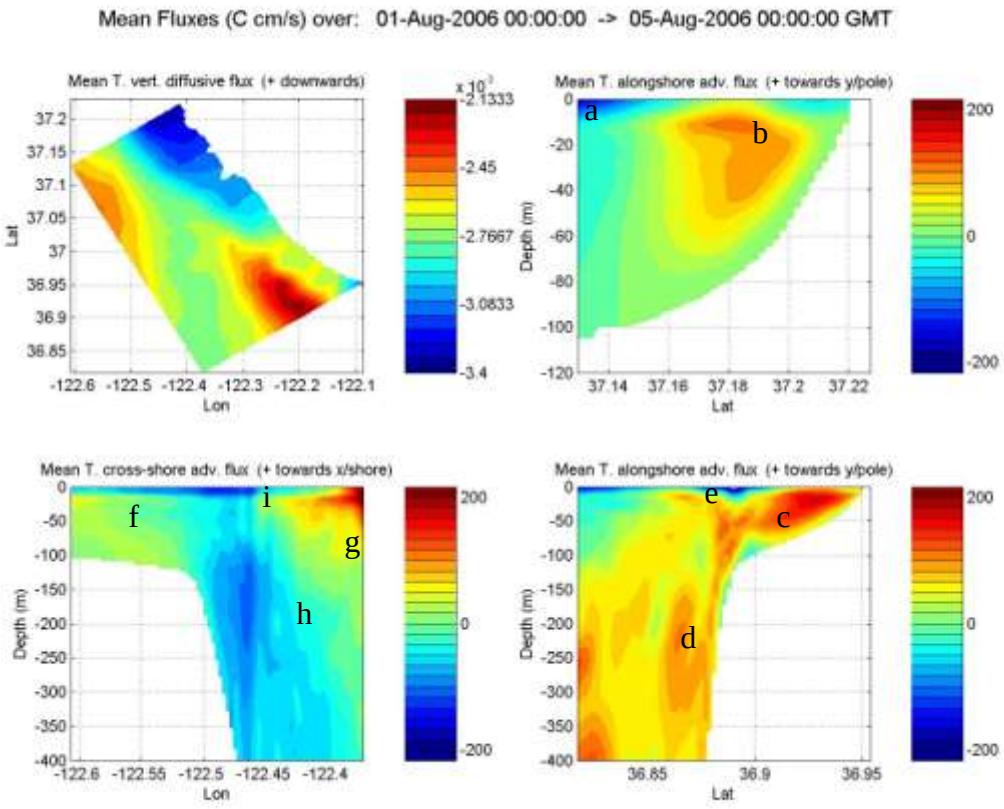

Figure 4-13: Heat Flux (C cm/s) through the Surface, North, South, and West Sections starting in Upper Left and going Clockwise for Run 12.

This run confirms the theory that data assimilation is important for initialization as this run does not resemble the baseline, but that tides are not a significant factor since this run resembles more closely the run with no data assimilation but tides than the run with no tides but data assimilation.

4.2.13 No Data Assimilation After the Start of First Event, No Tidal Forcing After the Start of First Event (Run 13)

Based on the above figure, we expect the run with no data assimilation and no tides to more closely resemble the run with no data assimilation after the first event than the run with no tides after the first event or the baseline. The results match this expectation. Feature (c) matches the baseline but is stronger, while all other features more closely resemble Run 8. However, the heat flux at (f) is much smaller and (g) is shallower.

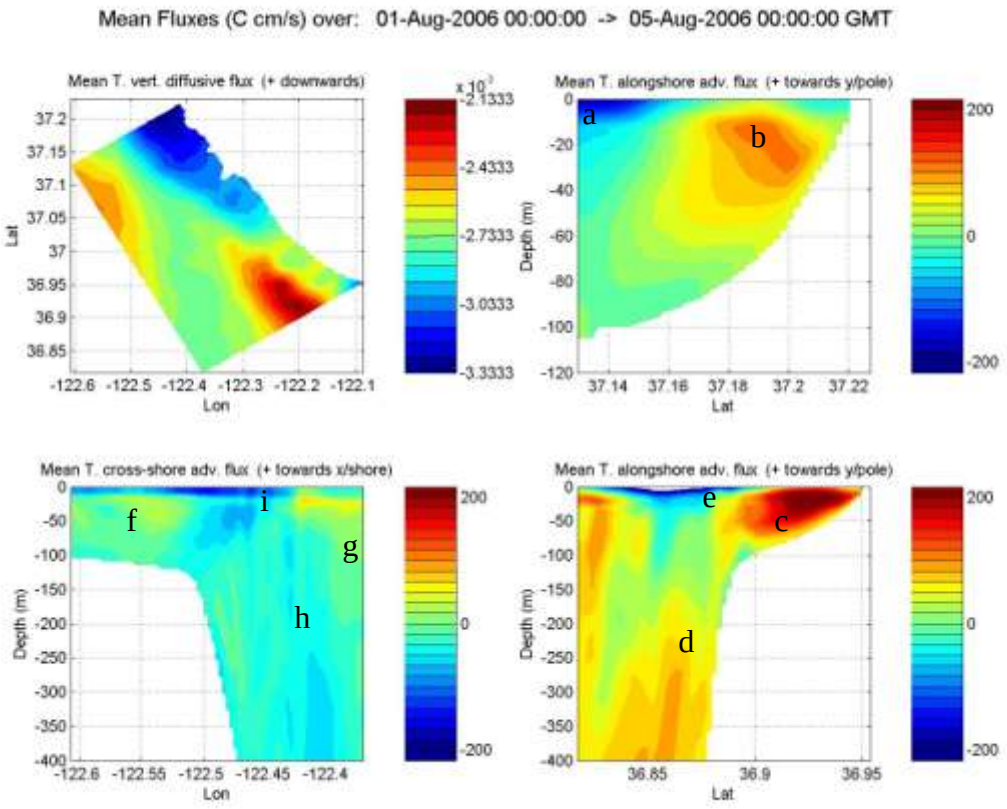

Figure 4-14: Heat Flux (C cm/s) through the Surface, North, South, and West Sections starting in Upper Left and going Clockwise for Run 13.

4.2.14 Summary

In conclusion, we completed a sensitivity study of the time-averaged lateral and surface heat fluxes for the Monterey region during MB06, focusing on the first upwelling event. Our simulations varied the surface forcings (wind, heat, evaporation minus precipitation, radiation), data assimilation, and tidal forcing. We found that the most important factors in matching the baseline simulations were the wind forcing and data assimilation. Data assimilation is necessary so as to set the initial background field and offshore forcing of the Ano Nuevo region. Tidal forcing did not have a significant effect on the simulations. Therefore, in designing ocean models of upwelling, the wind forcing and data assimilation should be better tuned than the other surface or tidal forcings.

4.3 Volume-Averaged Time Rate of Change of Temperature during the First Event

In what follows, we examine the volume-averaged time rate of change of temperature and investigate the trends and fluctuations in heating or cooling during the first upwelling event in the same domain as examined in Sect 4.2 (refer to Fig 4-1). This corresponds to the left-hand side of equation 4-3. We refer the reader to Table 3-1 for the list of runs and sensitivity studies.

4.3.1 Baseline (Run 1)

The baseline simulation was run with all four surface forcings, tidal forcing, and data assimilation. We can see an overall warming trend during the first upwelling event. The spikes in the temperature are due to tides and daily heating cycles and could also be possibly due to numerical artifacts of the data assimilation cycles. This later hypothesis is investigated in what follows.

It is very interesting to find out that this first upwelling event actually corresponds to a warming trend of the control volume we have chosen (around the Ano Nuevo shelf). The first two days correspond to a cooling (upwelling proper), but later the start of the relaxation event dominates the end of the wind forced response on the volume averaged.

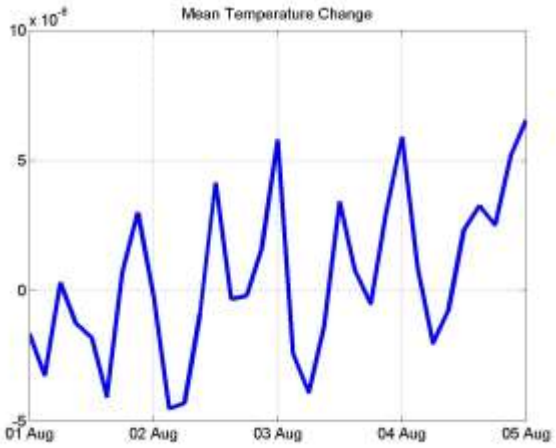

Figure 4-15: Volume-averaged time rate of change of temperature (K /s) for Run 1.

4.3.2 Only Wind Surface Forcing (Run 2)

For the run with only wind surface forcing, there is also an overall warming trend during the first event. The oscillations occur at the same times. The low points with only the wind forcing are lower than in the baseline. This, combined with the previous results, indicates that the warming trend is not driven by the surface heat, radiation or EMP flux but by internal ocean dynamics or data assimilation. Also, the fluctuations are either due to tides, to winds or to data assimilation artifacts.

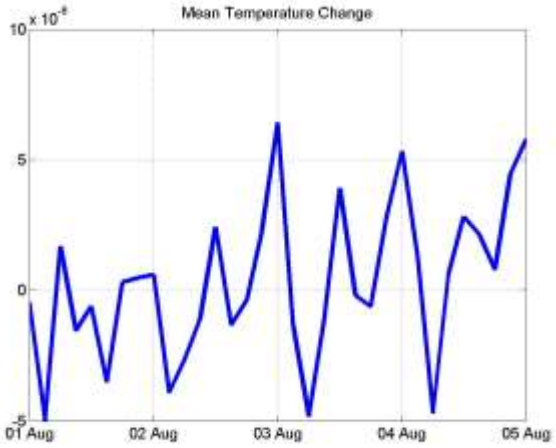

Figure 4-16: Volume-averaged time rate of change of temperature (K /s) for Run 2.

4.3.3 Only Heat Surface Forcing (Run 3)

The run with only heat surface forcing also oscillates at the same time as the baseline and shows an overall warming trend. The range of the mean temperature change is much smaller; the negative parts are much less negative. This indicates that the wind daily cycles are in part responsible for the amplitudes of the fluctuations.

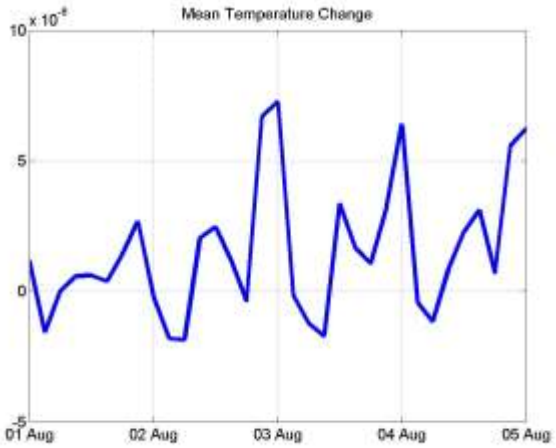

Figure 4-17: Volume-averaged time rate of change of temperature (K /s) for Run 3.

4.3.4 Only Evaporation Minus Precipitation (EMP) Surface Forcing (Run 4)

The run with only evaporation minus precipitation surface forcing also shows an overall warming trend. It oscillates many more times than the baseline for the first day and a half, and then it seems to match the trends of the baseline. These fast oscillations at the start are thus due to EMP, but they are overpowered or compensated by the wind and heat flux when these two forcings are turned on.

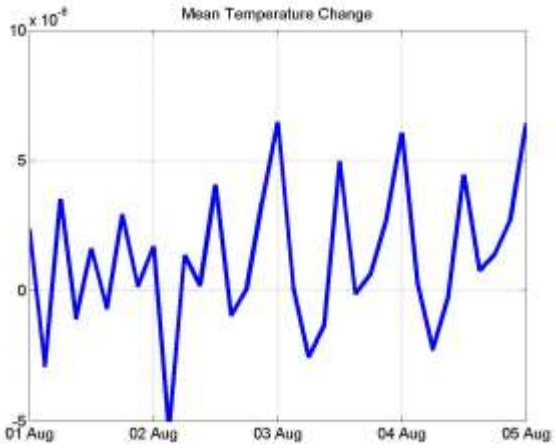

Figure 4-18: Volume-averaged time rate of change of temperature (K /s) for Run 4.

4.3.5 Only Short-wave Radiation Surface Forcing (Run 5)

The run with only short-wave radiation surface forcing starts off around zero and with many oscillations. After the first day, the number of oscillations decreases but the spikes, especially the peaks, are more pronounced.

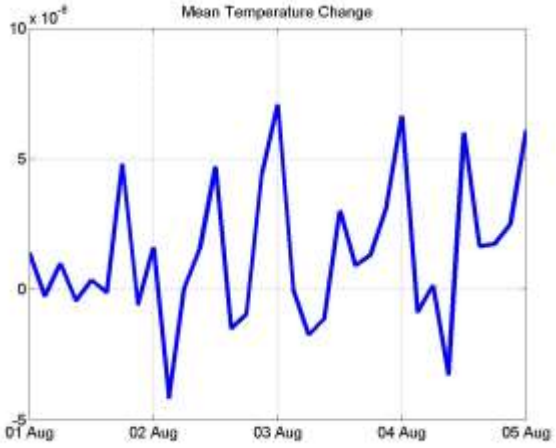

Figure 4-19: Volume-averaged time rate of change of temperature (K /s) for Run 5.

4.3.6 No Surface Forcing (Run 6)

The mean temperature change for the run with no surface forcing is identical to the run with only radiation forcing. This is normal because in the version of the model

used in this study, the short-wave radiation forcing is not modeled to affect the temperature field.

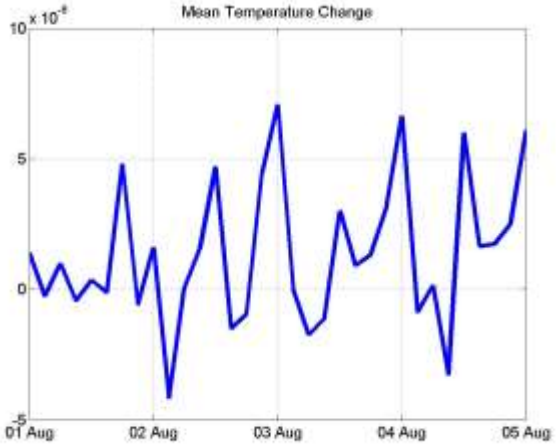

Figure 4-20: Volume-averaged time rate of change of temperature (K /s) for Run 6.

4.3.7 No Data Assimilation (Run 7)

The mean temperature change for event 1 for the run with no data assimilation is different from the baseline in frequency and amplitude, although there still is a general upward trend. The frequency is higher for the first two days than the last two days. The timing of the maxima is earlier than in the baseline run.

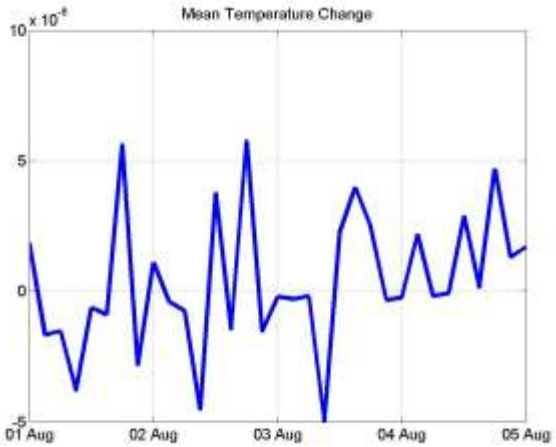

Figure 4-21: Volume-averaged time rate of change of temperature (K /s) for Run 7.

4.3.8 No Data Assimilation After the Start of the First Event (Run 8)

The mean temperature change for the run with no data assimilation after the first event more closely resembles the baseline than the run with no data assimilation, especially for the first day. This again shows the existence of a predictability limit. The mean temperature change increases overall throughout the first upwelling event. The timing of the largest temperature change in run 8 is between the spikes in the baseline.

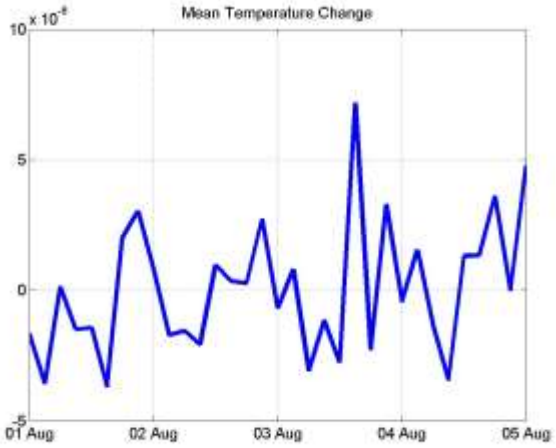

Figure 4-22: Volume-averaged time rate of change of temperature (K /s) for Run 8.

4.3.9 No Surface Forcing, No Data Assimilation (Run 9)

The run with no surface forcing and no data assimilation shows a roughly constant temperature change with a larger change of amplitude between the peaks and valleys than any other run until August 4th-5th.

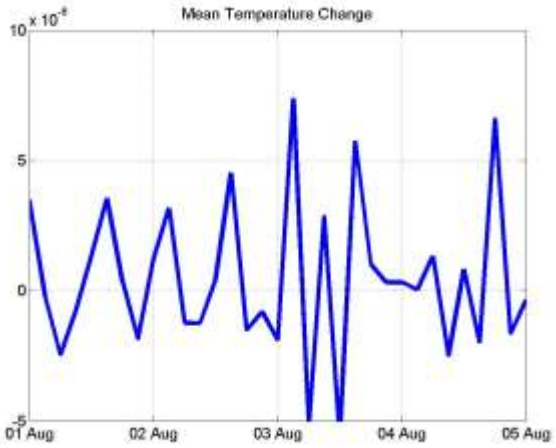

Figure 4-23: Volume-averaged time rate of change of temperature (K /s) for Run 9.

4.3.10 No Tidal Forcing (Run 10)

The run with no tidal forcing has less extreme peaks and valleys as expected. The oscillations that remain can possibly be explained by data assimilation cycles, or more likely daily temperature fluctuations due to solar heating. The mean temperature change shows an upward trend during the upwelling event. A conclusion of this run, when combined with the results of the runs already discussed, is that the daily oscillations in the baseline run are mainly due to tides and also due a bit to wind stress.

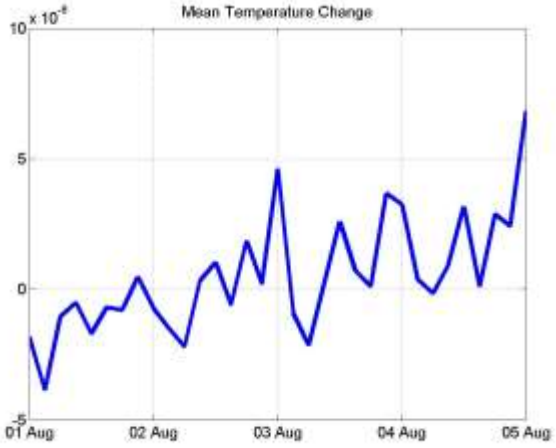

Figure 4-24: Volume-averaged time rate of change of temperature (K /s) for Run 10.

4.3.11 No Tidal Forcing After the Start of the First Event (Run 11)

The results of the mean temperature change for the run with no tidal forcing after the first event also show a general upward trend. Initially, this run looks more like the baseline than the run with no tides; however, afterwards it is closer to the latter run, with fewer fluctuations.

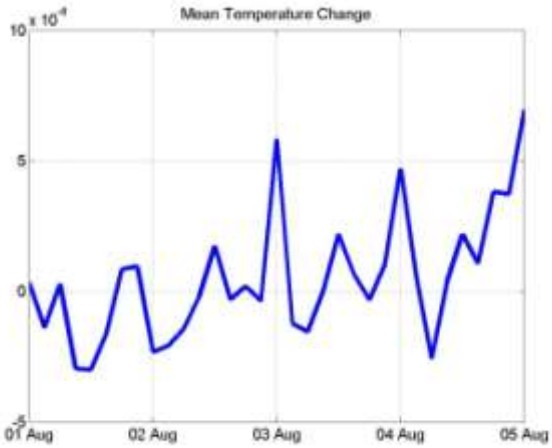

Figure 4-25: Volume-averaged time rate of change of temperature (K /s) for Run 11.

4.3.12 No Data Assimilation, No Tides (Run 12)

The run with no data assimilation and no tides shows variability similar to the run with no tides, indicating that the variability in the baseline is controlled by tides. There are some high frequency oscillations that are likely due to internal oscillations and other surface forcing.

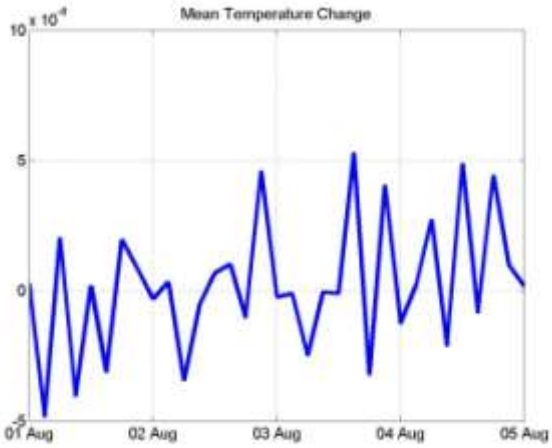

Figure 4-26: Volume-averaged time rate of change of temperature (K /s) for Run 12.

4.3.13 No Data Assimilation After the Start of the First Event, No Tidal Forcing After the Start of the First Event (Run 13)

The volume-averaged time rate of change of temperature for the run with no data assimilation after the start of the first event and no tidal forcing after the start of the first event does not show as strong as an upward trend as that in the runs with data assimilation. There are high frequency fluctuations, especially after the first day, which are most likely driven by tidal energy that is dissipated in faster scale motions such as internal oscillations and tides and waves.

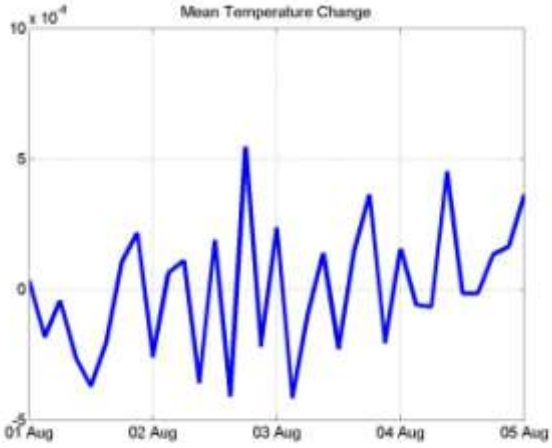

Figure 4-27: Volume-averaged time rate of change of temperature (K /s) for Run 13.

4.3.14 Conclusions

The volume-averaged time rate of change of temperature showed a warming trend during the first event. The fluctuations were due to tides, wind, and data assimilation artifacts. The tidal forcing is very important to the fluctuations in the volume-averaged time rate of change of temperature, while they were not a key parameter in the time-averaged heat fluxes.

5 Conclusion

In this work, we used a data-assimilative modeling approach using the MIT-MSEAS system to study upwelling events in Monterey Bay. We focused on the first upwelling event from August 1 0:00Z to August 5 0:00Z during MB06. To determine the major factors that control the dynamics of this event, we varied the surface forcings (wind stress, heat flux, evaporation minus precipitation, short-wave radiation), tidal forcing, and data assimilation. In addition to studying the full ocean fields from these varied simulations, we also compared the time-averaged fluxes at the boundaries of a control volume centered on the Ano Nuevo shelf as well as the volume-averaged rate-of-changes over that same control volume.

From the sensitivity simulations and the comparisons of ocean field evolutions, we were able to conclude that the wind stress was an important driver of the upwelling dynamics. There was still upwelling present when we ran the simulation with only surface heat fluxes, although the upwelling was reduced. In fact, this upwelling was then found to be an artifact of the data assimilation, which is in some sense also a good thing, i.e. the data assimilation works (and corrects model biases in this case, the lack of wind stress forcing). Data assimilation affects the small domain from the interior but also affects it from the inflows of data assimilated in the large domain. This is because by the time the first event starts, the initialization survey was not yet completed. Wind stress forcing and data assimilation had the largest difference on whether there was upwelling and the shape of the upwelling event; altering the other surface forcing and tidal forcings did not have as large an impact on the ocean field evolutions.

These conclusions were supported when we examined the heat fluxes at the surface boundaries of a control volume centered around the Ano Nuevo shelf. Upwelled waters advected offshore were only present in the runs with wind stress forcing. Data assimilation was required for accurate short predictions since without synoptic data, atmospheric forcing could sufficiently correct the fields at depth. Tidal forcing did not play a significant role on the time-averaged fluxes when compared to wind stress forcing and data assimilation.

We also examined the volume-averaged time rate of change of temperature for that same domain centered around Ano Nuevo for the first upwelling event. There was an overall warming trend of the control volume, with the first two days corresponding to a cooling (upwelling proper) while the start of the relaxation event dominated the end of the wind forced response. Here we found that the fluctuations

were mainly due to winds, tides, and data assimilation. Tidal forcing seemed the most dominant factor in these high-frequency fluctuations.

Future work would verify these results for the other upwelling and relaxation events and other control volumes during MB06. Our quick study of the second event clearly confirms that there are different types of upwelling events in the region. We would also examine the salt balances. Another area of investigation would involve investigating the Lagrangian point of view by following particles, water-masses, or Lagrangian Coherent Structures. From the results of these runs, we could create better four-dimensional geophysical fluid dynamics characterizations of upwelling and relaxation events in the region.

6 References

Argawal, A and Lermusiaux, P.F.J. (2010). Statistical field estimation for complex coastal regions and archipelagos. *Ocean Modeling*, in preparation.

Cushman-Roisin, B. and Beckers, J.M. (2010). *Introduction to geophysical fluid dynamics: Physical and Numerical Aspects.* Academic Press.

Delsole, T., and Tippett, M.K. (2007). Predictability: Recent insights from information theory. *Review of Geophysics*, 45(RG4002).

Dever, E.P. and Lentz, S.J. (1994). Heat and salt balances over the northern California shelf in winter and spring. *Journal of Geophysical Research*. 99(C8): 16001-16017.

Doyle, J.D., Jiang, Q., Chao, Y., and Farrara, J. (2009). High-resolution real-time modeling of the marine atmospheric boundary layer in support of the AOSNII field campaign. *Deep-Sea Research II*, 56: 127-148.

Drake, P.T., McManus, M.A., and Storlazzi, C.D. (2005). Local wind forcing of the Monterey Bay area inner shelf. *Continental Shelf Research*, 25: 397-417.

Gangopadhyay, A., Lermusiaux, P.F.J., Robinson, A.R., and Rosenfeld, L. (2010a). On the multi-scale synoptic nature of the California Current System. *Ocean Modeling*, to be submitted.

Gangopadhyay, A., Lermusiaux, P. F. J., Leslie, W.G., Haley, P.J., Robinson, A.R., Calado, L., Kim, H.S., and Rosenfeld, L. (2010b). Development of a Feature-Oriented Regional Modeling System (FORMS) for the California Current System, *Ocean Modeling*, to be submitted.

Haley, P.J., Lermusiaux, P.F.J., Robinson, A.R., Leslie, W.G., Logoutov, O., Cossarini, G., Liang, X.S., Moreno, P., Ramp, S.R., Doyle, J.D., Bellingham, J., Chavez, F., and Johnston, S. (2009). Forecasting and reanalysis in the Monterey Bay/California Current region for the Autonomous Ocean Sampling Network-II experiment. *Deep-Sea Research II*, 56: 127-148.

Haley, P.J., and Lermusiaux, P.F.J. (2010). Multiscale two-way embedding schemes for free-surface primitive-equations in the "Multidisciplinary Simulation,

Estimation and Assimilation System" (MSEAS). *Ocean Dynamics*, in preparation.

Heubel, E. (2008). Parameter estimation and adaptive modeling studies in ocean mixing. *SM Thesis, Massachusetts Institute of Technology*.

Kelly, K.A. (1985). The influence of winds and topography on the sea surface temperature patterns over the Northern California Slope. *Journal of Geophysical Research*, 90(C6): 11783-11798.

Largier, J.L., Magnell, B.A., and Winant, C.D. (1993). Subtidal circulation over the northern California shelf. *Journal of Geophysical Research*, 98(C10): 18417-18179.

Lentz, S.J. (1987). A heat budget for the Northern California Shelf during CODE 2. *Journal of Geophysical Research*, 92(C13): 14491-14509.

Lermusiaux, P.F.J. (1999). Estimation and study of mesoscale variability in the strait of Sicily. *Dynamics of Atmospheres and Oceans*, 29: 255-303.

Lermusiaux, P.F.J, Robinson, A.R., Haley, P.J., and Leslie, W.G. (2002). Filtering and smoothing via Error Subspace Statistical Estimation. *The Oceans 2002 MTS/IEEE*, Holland Publications, 795-802.

Lermusiaux, P.F.J. (2006). Uncertainty Estimation and Prediction for Interdisciplinary Ocean Dynamics. *Journal of Computational Physics, Special Issue on "Uncertainty Quantification,"* ed. Glimm, J and Karniadakis, G, 176-199.

Lermusiaux, P.F.J. (2007). Adaptive sampling, adaptive data assimilation and adaptive modeling. *Physica D., Special issue on "Mathematical Issues and Challenges in Data Assimilation for Geophysical Systems: Interdisciplinary Perspectives*." Ed. Jones, C.K.R.T. and Ide, K., 230: 172-196.

Lermusiaux, P.F.J, and Xu, J. (2010). Coupled Ocean-Acoustic prediction of transmission loss in a continental shelfbreak region: predictive skill, uncertainty quantification and dynamical sensitivities. *IEEE Transactions, Journal of Oceanic Engineering*, submitted.

Ramp, S.R., Davis, R.E., Leonard, N.E., Shulman, I., Chao, Y., Robinson, A.R., Marsden, J., Lermusiaux, P.F.J., Fratantoni, D.M., Paduan, J.D., Chavez, F.P., Bahr, F.L., Liang, S., Leslie, W., and Li, Z. (2009). Preparing to predict: The Second Autonomous Ocean Sampling Network (AOSN-II) experiment in the Monterey Bay. *Deep- Sea Research II*, 56: 68-86.

Rosenfeld, L.K., Schwind, F.B., Garfield, N., and Tracy, D.E. (1994). Bifurcated flow from an upwelling center: a cold water source for Monterey Bay. *Continental Shelf Research*, 14(9): 931-964.

Rosenfeld, L., Shulman, I., Cook, M., Paduan, J., and Shulman, L. (2009). Methodology for a regional tidal model evaluation, with application to central California. *Deep- Sea Research II*, 56: 199-218.

Rudnick, D.L. and Davis, R. E. (1988). Mass and heat budgets on the Northern California Continental Shelf. *Journal of Geophysical Research*, 93(C11): 14013-14024.

Sapsis, T.P. and Lermusiaux, P.F.J. (2009). Dynamically orthogonal field equations for continuous stochastic dynamical systems. *Physica D*, 238: 2347-2360.

Send, U., Beardsley, R.C., and Winant, C.D. (1987). Relaxation from upwelling in the Coast Ocean Dynamics Experiment. *Journal of Geophysical Research*, 92(C2): 1683-1698.

Shulman, I., Rowley, C., Anderson, S., DeRada, S., Kindle, J., Martin, P., Doyle, J., Cummings, J., Ramp, S., Chavez, F., Fratantoni, D., and Davis, R. (2009). Impact of glider data assimilation on the Monterey Bay model. *Deep- Sea Research II*, 56: 188-198.

Storlazzi, C.D., McManus, M.A., and Figurski, J.D. (2003). Long-term, high frequency current and temperature measurements along central California: insights into upwelling/relaxation and internal waves on the inner shelf. *Continental Shelf Research*, 23: 901-918.

Tian, R.C., Lermusiaux, P.F.J., McCarthy, J.J., and Robinson, A.R. (2008). A generalized prognostic model of marine biogeochemical-ecosystem dynamics: Structure, parameterization and adaptive modeling. *Harvard Reports in Physical/Interdisciplinary Ocean Science*, 67:1-65.

Wang, X., Chao, Y., Dong, C., Farrara, J., Li, Z., McWilliams, J.C., Paduan, J.D., and Rosenfeld, L.K. (2009). Modeling tides in Monterey Bay, California. *Deep-Sea Research*, 56: 219-231.